AD-A172 783 AN INVESTIGATION OF A PHASE CONJUGATE RESONATOR BASED ON STIMULATED BRILL... (U) AIR FORCE INST OF TECH WRIGHT-PATTERSON AFB OH SCHOOL OF ENGI... V C ESCH 1/1

UNCLASSIFIED MAR 86 AFIT/GEP/ENP/85D-11 F/G 20/6 NL

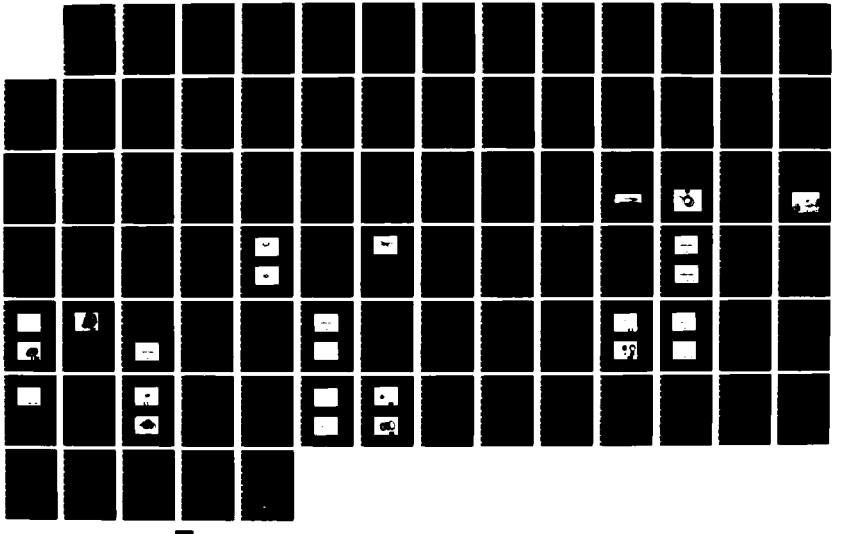

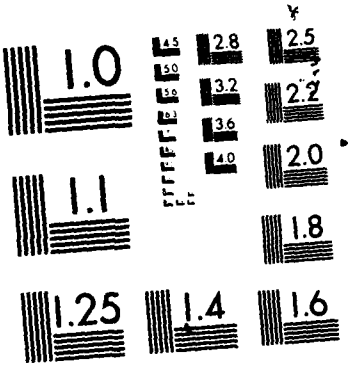

AN INVESTIGATION OF A PHASE CONJUGATE RESONATOR BASED ON STIMULATED BRILLOUIN SCATTERING

THESIS

Victor C. Esch
First Lieutenant, USAF

AFIT/GEP/ENP/85D-11

DEPARTMENT OF THE AIR FORCE
AIR UNIVERSITY
AIR FORCE INSTITUTE OF TECHNOLOGY

Wright-Patterson Air Force Base, Ohio

AN INVESTIGATION OF A PHASE CONJUGATE RESONATOR BASED ON STIMULATED BRILLOUIN SCATTERING

THESIS

Victor C. Esch
First Lieutenant, USAF

AFIT/GEP/ENP/85D-11

AFIT/GEP/ENP/85D-11

AN INVESTIGATION OF A PHASE COJUGATE RESONATOR BASED ON STIMULATED BRILLOUIN SCATTERING

THESIS

Presented to the Faculty of the School of Engineering

of the Air Force Institute of Technology

Air University

In Partial Fulfillment of the

Requirements for the Degree of

Master of Science in Engineering Physics

Victor C. Esch, B.S.

First Lieutenant, USAF

March 1986

Acknowledgments

I would like to acknowledge the support given to me in my scholastic endeavors, in particular by the Avionics Laboratory Electronic Technology Division and Electro-Optic Technology Branch. At the Air Force Institute of Technology I would like to thank Dr. W.B. Roh for his support as my thesis advisor, and all the other instructors for the knowledge they imparted to me.

I am most grateful for the support, tutelage, patience, and encouragement of Don 'Sandy' Smith and Joe Brandelik. They have each endured many hours of ignorant questions and nearly as many hours argument. With the practical and theoretical information that they possess, a small fraction of which I procured, the classes I took at AFIT were greatly supplemented.

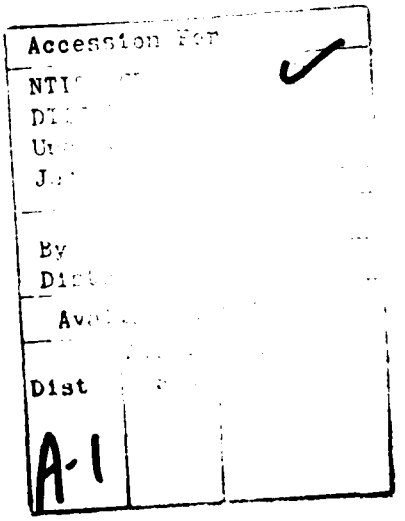

Table of Contents

List of Figures

List of Tables

Abstract

A phase conjugate resonator (PCR) using stimulated Brillouin scattering (SBS) was investigated. Carbon disulfide, in a waveguide tube, was used as the nonlinear medium. A collinear startup resonator was employed, and output was obtained by cavity dumping the phase conjugate resonator.

The performance of the PCR was optimized through the use of various etalon elements, including resonant reflectors. Aberrators and cavity misalignment were used to test the fault tolerance of the PCR.

The PCR compensated well for induced faults with respect to energy output, but beam quality was, in general, degraded with the SBS process. The large SBS frequency shift of carbon disulfide hurt the performance of the PCR.

Phase Conjugate Resonator

I. Introduction

Background.

The United States Air Force has a continuing need for high efficiency solid state laser oscillators. These oscillators must be able to withstand extreme environmental stress without degradation. The current laser systems of choice are based on the Neodymium ion. These systems, whether they are low power single oscillator, or high power oscillator-amplifier, rely on a high beam quality, stable, and efficient resonator. Up to the present, beam quality and stability has dictated the use of other than optimal mode volume utilization. This detrimentally affects efficiency. Phase conjugation might offer a way to produce higher efficiency laser resonators and, with the proper transverse mode control, maintain high beam quality. Equally important, or in some cases more so, phase conjugation may vastly increase the fault tolerance of a laser resonator.

Problem Definition.

The objective of this thesis was to construct an operational phase conjugate resonator and to characterize it. The behavior of the resonator with respect to beam quality, spectral content, and output energy was investigated, with and without cavity misalignment and intracavity aberrators.

Approach.

In order to produce a phase conjugate resonator (PCR) using stimulated Brillouin scattering (SBS) a laser oscillator must already exist so that the SBS can be initiated. This initiating laser oscillator, called the startup resonator (SUR), can be situated in many different configurations. For this experiment a collinear SUR was employed (see Figure 1).

The SUR was simply a Q-switched laser with the fluence from the output coupler focused into the SBS medium, in this case carbon disulfide (CS_2) in a pyrex cell. As the Q-switched pulse built up in the SUR the intensity into the cell increased and SBS was induced. The net reflectivity of the output coupler end of the laser oscillator increased dynamically; increased SBS reflectivity caused increased intracavity fluence, and the increased fluence produced more SBS reflectivity. Through this process a PCR was produced.

Ideally the energy in the PCR cavity should be switched out, or cavity dumped, when the intracavity fluence reaches its peak value. The electronics to initiate the cavity dump switch via an intracavity fluence detector was not available. Instead, the cavity dump switch driver was directly triggered by the Q-switch driver with the shortest delay practical (dictated by the shortest coax lead and the driver's response time). This gave the best achievable experimental performance.

Once the PCR was operational efforts were made to optimize its performance given the available equipment. The effects of the spectral properties of the SUR on the PCR performance were investigated to the

extent that only qualitative observations could be made concerning the spectral content of the PCR or SUR output. The increase in cavity dumped energy could be quantified, and was enhanced by employing etalon elements to narrow the spectral output of the SUR. The narrowing of the SUR was found to be the primary means to increase the phase conjugate reflectivity, and thus improve PCR performance. The effect of cavity aperturing was also investigated.

To test the fault tolerance of the PCR the SUR was alternately aberrated and misaligned. The aberrators were in the form of a glass microscope slide and a wire screen. To misalign the cavity the SUR output coupler was translated 4 miliradians in the axis of cavity polarization. The PCR demonstrated the ability to compensate for the introduced faults with respect to cavity dumped energy, but not for beam quality.

The output of the PCR, and SUR, was examined by various diagnostic equipment. Characterization included spatial beam profile, temporal pulse shape, pulse energy, and spectral content. The facilitation of these measurements proved to be as time consuming as the actual PCR setup, neither of which worked faultlessly.

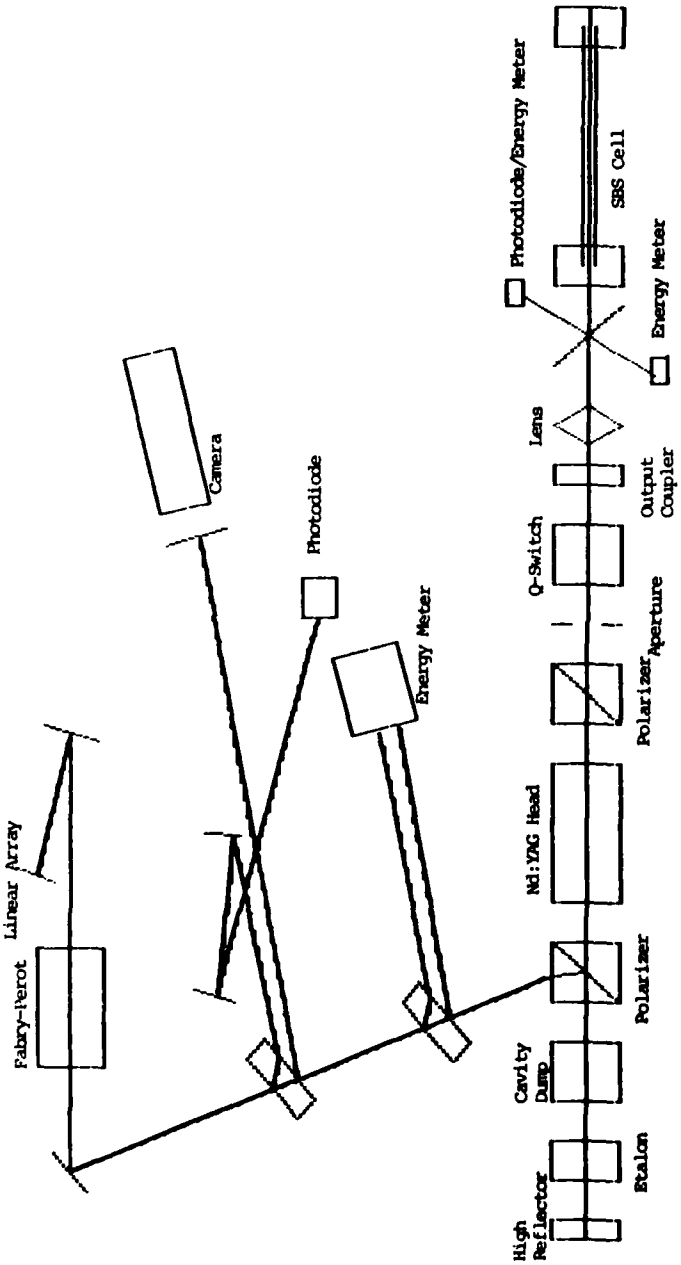

Figure 1 Schematic diagram of the experimental setup used for the phase conjugate resonator.

II. Theory.

The following is a presentation of the theory applicable to a phase conjugate resonator. The general theory of stimulated Brilloun scattering will be dealt with first, followed by that of the transverse modes of a 'generic' form of a PCR. In as much as the theory for the particular PCR constructed for this thesis has not yet been developed, the expected results for this case must be extrapolated from that theory that is now available. A complete Hermite-Gaussian transverse mode or longitudinal mode analysis is beyond the scope of this thesis.

Stimulated Brillouin Scattering.

Brillouin scattering involves the coupling of light and acoustic waves. This phenomena was investigated as early as 1922 by, of course, Brillouin. Stimulated Brillouin scattering occurs when the acoustic waves are themselves generated by the incident optical waves through a nonlinear interaction. The following classical derivation follows the approach given by Yariv (21:491), and the argument that demonstrates that the scattered wave is phase conjugate is from Zel'dovich et al. (23:1120).

If a small volume dx dy dz of a fluid is subject to a large electric field the fluid may be put under strain. If the displacement from equilibrium of some point x in the x direction is called u(x,t) then the one dimensional strain put on this point is

$$\frac{\partial u(x,t)}{\partial x} \tag{1}$$

The strain induced change in the dielectric constant may be related to

the strain through some constant

$$\delta\varepsilon = -\gamma \frac{\partial u}{\partial x} \tag{2}$$

where γ, the photoelastic constant, is determined experimentally for the fluid. Thus the stored electrostatic energy density is changed by $\frac{1}{2}\delta\varepsilon E^2$.

If the amount of the work done to produce the strain is equated to the increase in stored energy then

$$p\frac{\partial u}{\partial x} = \frac{1}{2}\delta\varepsilon E^2 \tag{3}$$

$$p = -\frac{1}{2}\gamma E^2 \tag{4}$$

where p is the pressure. The electrostrictive force acting on this volume in the positive x direction is

$$F = -\frac{\partial p}{\partial x} = \frac{\gamma}{2}\frac{\partial E^2}{\partial x} \tag{5}$$

The pertinent equation for a damped driven acoustic wave (15:44,129) is

$$-\eta\frac{\partial u}{\partial t} + T\frac{\partial^2 u}{\partial x^2} + \frac{\gamma}{2}\frac{\partial E^2}{\partial x} = \rho\frac{\partial^2 u}{\partial t^2} \tag{6}$$

where η is the acoustic loss constant, T is the bulk modulus and ρ is the mass density.

If a solution for u is assumed of the form

$$u(\vec{r},t) = \frac{1}{2}u_s(r_s)e^{i(\omega_s t - \vec{k}_s\cdot\vec{r})} + c.c. \tag{7}$$

where r_s is the distance along $\vec{k}_s$ the equation may be rewritten as

$$\left[(-\imath\eta\omega_s + \rho\omega_s^2)u_s(r_s) - T(k_s^2 u_s(r_s) + 2\imath k_s \frac{\partial u_s(r_s)}{\partial r}) \right] e^{\imath(\omega_s t - \vec{k}_s \cdot \vec{r})} = -\frac{\partial E^2}{\partial r_s} \quad (8)$$

where $\frac{\partial^2 u_s(r_s)}{\partial r^2}$ has been neglected as very small and x has been replaced with r_s .

A form for the two electric field plane waves traveling in arbitrary directions is assumed,

$$\vec{E}_1(\vec{r},t) = \frac{1}{2} E_1(r_1) e^{\imath(\omega_1 t - \vec{k}_1 \cdot \vec{r})} + c.c. \quad (9)$$

$$\vec{E}_2(\vec{r},t) = \frac{1}{2} E_2(r_s) e^{\imath(\omega_2 t - \vec{k}_2 \cdot \vec{r})} + c.c. \quad (10)$$

eq (8) may be written

$$\left[(-\imath\eta\omega_s + \rho\omega_s^2)u_s(r_s) - T(k_s^2 u_s(r_s) + 2\imath k_s \frac{\partial u_s(r_s)}{\partial r}) \right] e^{\imath(\omega_s t - \vec{k}_s \cdot \vec{r})} + c.c.$$

$$= -\frac{\gamma}{q} \frac{\partial}{\partial r_s} \left(E_2(r_s) E_1^*(r_1) e^{\imath((\omega_2 - \omega_1)t - (\vec{k}_2 - \vec{k}_1)\cdot\vec{r})} + c.c. \right) \quad (11)$$

If the exponential frequency terms in equation (11) are required to fulfill

$$\omega_s = \omega_2 - \omega_1 \quad (12)$$

and

$$\vec{k}_s = \vec{k}_2 - \vec{k}_1 \quad (13)$$

eq (11) may now be written as

$$\left(-\frac{\imath\eta\omega_s}{\rho} + \omega_s^2 - \frac{Tk_s}{\rho} \right) u_s(r_s) - \frac{T}{\rho} 2\imath k_s \frac{\partial u_s(r_s)}{\partial r} = \frac{\imath\gamma k_s}{4\rho} E_2(r_s) E_1^*(r_1) \quad (14)$$

Now using $v_s^2 = \frac{T}{\rho}$ and rearranging terms,

$$v_s^2 2\imath k_s \frac{\partial u_s(r_s)}{\partial r_s} + (v_s^2 k_s^2 - \omega_s^2 + \frac{\imath\eta\omega_s}{\rho}) u_s(r_s) = \frac{\imath k_s \gamma}{4\rho} E_2(r_s) E_1^*(r_1) \quad (15)$$

The equations governing the plane electric fields may be derived from Maxwell's equations. Starting with the wave equation

$$\nabla^2 \vec{E} = \mu \frac{\partial^2 \vec{D}}{\partial t^2} \quad (16)$$

Substituting $\vec{D}=\varepsilon\vec{E}+\vec{P}_{NL}$, where ϵ includes the linear polarization, and $\vec{P}_{NL}$ is the nonlinear polarization, eq (16) becomes

$$\nabla^2\vec{E} = \mu\varepsilon\frac{\partial^2\vec{E}}{\partial t^2} + \mu\frac{\partial^2\vec{P}_{NL}}{\partial t^2} \tag{17}$$

Using eq (9) for $\vec{E}$

$$-\tfrac{1}{2}\left[E_1(r_1)k_1^2 + 2ik_1\cdot\nabla E_1(r_1) - \nabla^2 E_1(r_1)\right]e^{i(\omega_1 t-\vec{k}_1\cdot\vec{r})} + c.c.$$

$$= -\mu\varepsilon\frac{\omega_1^2}{2}E_1(r_1)e^{i(\omega_1 t-\vec{k}_1\cdot\vec{r})} + c.c. + \mu\frac{\partial^2\vec{P}_{NL}}{\partial t^2} \tag{18}$$

If $\nabla^2 E_1(r_1)$ is ignored as very small eq (18) may be rearranged and written

$$k_1\frac{dE_1(r_1)}{dr_1}e^{i(\omega_1 t-\vec{k}_1\cdot\vec{r})} + c.c. = i\mu\frac{\partial^2\vec{P}_{NL}}{\partial t^2} \tag{19}$$

The term on the right of eq (19) contains P_{NL} (associated with E_1). This P_{NL} is the additional polarization caused by the E field produced acoustic wave. Recalling $\vec{P}=\varepsilon\vec{E}$

$$\vec{P}_{NL} = \delta\varepsilon\vec{E} \tag{20}$$

and with eq (2)

$$P_{NL} = -\gamma E(\vec{r},t)\frac{\partial u(\vec{r},t)}{\partial r_3} \tag{21}$$

Thus eq (19) becomes

$$k_1\frac{dE_1(r_1)}{dr_1}e^{i(\omega_1 t-\vec{k}_1\cdot\vec{r})} + c.c. = i\mu\frac{\partial^2}{\partial t^2}\left[-\gamma E(\vec{r},t)\frac{\partial u(\vec{r},t)}{\partial r_3}\right] \tag{22}$$

Examining the frequency terms on the left of eq (22) (ω_1), and those present on the right in the form of E (ω_1 or ω_3) and $u(\vec{r},t)$ (ω_3) it is seen that in order to have synchronous driving, only terms of ($\omega_3-\omega_3$)

are allowed on the right of eq (22). That is $\pm\imath\omega_1=\pm\imath(\omega_3-\omega_2)$. Now eq (22) may be written as

$$k_1\frac{dE_1(r_1)}{dr_1}e^{\imath(\omega_1 t-\bar{k}_1\cdot\bar{r})}=\frac{\imath\mu}{4}\frac{\partial^2}{\partial t^2}\left\{-\gamma E_2(r_2)e^{\imath(\omega_2 t-\bar{k}_2\cdot\bar{r})}\cdot\frac{\partial}{\partial r_3}\left[u_3^*(r_3)e^{-\imath(\omega_3 t-\bar{k}_3\cdot\bar{r})}\right]\right\} \quad (23)$$

Performing the derivatives and assuming $|k_3u_3^*| >> \left|\frac{\partial u_3}{\partial r_3}\right|$

$$\frac{dE_1(r_1)}{dr_1}=-\frac{\omega_1^2\gamma\mu k_3}{4k_1}E_2(r_2)u_3^*(r_3) \quad (24)$$

Up to this point any loss at frequency ω_1 has been ignored. To account for this loss a factor $-\alpha E_1/2$ is added phenomenologically, producing

$$\frac{dE_1(r_1)}{dr_1}=-\frac{\omega_1^2\gamma\mu k_3}{4k_1}E_2(r_2)u_3^*(r_3)-\frac{\alpha E_1(r_1)}{2} \quad (25)$$

where $\alpha=\sigma\mu_0\sqrt{\frac{\mu_0}{\varepsilon}}$ and σ is the conductivity.

A completely analogous derivation can be performed for $E_2(r_2)$. Summarizing the pertinent equations

$$v_3^2 2\imath k_3\frac{\partial u_3(r_3)}{\partial r_3}+(v_3^2k_3^2-\omega_3^2+\frac{\imath\eta\omega_3}{\rho})u_3(r_3)=\frac{\imath k_3\gamma}{4\rho}E_2(r_2)E_1^*(r_1) \quad (26)$$

$$\frac{dE_1(r_1)}{dr_1}=-\frac{\omega_1^2\gamma\mu k_3}{4k_1}E_2(r_2)u_3^*(r_3)-\frac{\alpha E_1(r_1)}{2} \quad (27)$$

$$\frac{dE_2(r_2)}{dr_2}=-\frac{\omega_2^2\gamma\mu k_3}{4k_2}E_1(r_1)u_3^*(r_3)-\frac{\alpha E_2(r_2)}{2} \quad (28)$$

Now the specialized case of stimulated Brillouin scattering is considered, where an incident field at ω_2 generates an acoustic field at ω_3, and thus the scattered field at ω_1. First it is assumed that the pump field E_2 is not depleted, or E_2 =constant. Also it is assumed that the acoustic dispersion is that of free and lossless space, or $\omega_3=k_3v_3$. The equations to be considered are now

$$\frac{du_s(r_s)}{dr_s} = \frac{-\eta u_s(r_s)}{2\rho v_s} - \frac{\gamma}{8\rho v_s^2} E_2(r_2) E_1^*(r_1) \qquad (29)$$

and

$$\frac{dE_1^*(r_1)}{dr_1} = -\frac{\alpha E_1^*(r_1)}{2} - \frac{\gamma k_1 k_s}{4\epsilon_1} E_2^*(r_2) u_s(r_s) \qquad (30)$$

where, again, r_1 and r_s are the distances measured along $\vec{k}_1$ and $\vec{k}_s$ respectively. This complexity in two direction variables may be alleviated by transforming to the coordinate ξ as in Figure 2. By using $r_s = r_2 = q = \xi \cos\theta$, eq (29) and (30) may be written

$$\frac{du_s(q)}{dq} = \frac{-\eta u_s(q)}{2\rho v_s} - \frac{\gamma}{8\rho v_s^2} E_2(q) E_1^*(q) \qquad (31)$$

$$dE_1^*(q) = -\frac{\alpha E_1^*(q)}{2} - \frac{\gamma k_1 k_s}{4\epsilon_1} E_2(q) u_s(q) \qquad (32)$$

If solutions for the growth rate are assumed in the form

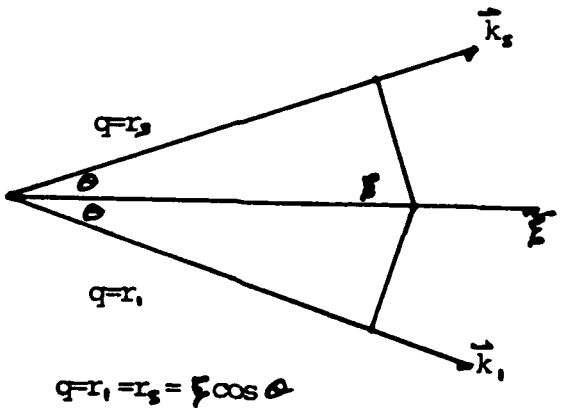

Figure 2 Relationship of r_1 and r_s through q (21:495)

$$u_s(q) = u_s^{\circ} e^{gq} \tag{33}$$

$$E_1^*(q) = E_1^{o*} e^{gq} \tag{34}$$

the result for g may be found by determinentally solving eq (31) and (32) after substituting eq (33) and (34). Thus,

$$g = -\frac{1}{4}(\alpha_s + \alpha) + \frac{1}{4}\left[(\alpha_s+\alpha)^2 - 4\left(\alpha_s\alpha - \frac{k_1 k_s \gamma^2 |E_2|^2}{8\rho_0 v_1 v_s^2}\right)\right]^{1/2} \tag{35}$$

where α_s is the acoustic loss term in the form of $\alpha_s = \frac{-\eta}{\rho v_s}$.

It can be seen from the eq (13), here repeated,

$$\vec{k}_s = \vec{k}_2 - \vec{k}_1$$

that $k_s = 2k_2 \sin\theta$, where 2θ subtends $\vec{k}_2$ and $\vec{k}_1$, and $|\vec{k}_2| \simeq |k_1|$. This is the same as the Bragg scattering condition. Thus the maximum gain occurs for backward scattering, or $\theta = \pi/2$.

To demonstrate that the scattered field is phase conjugate (23:1120), eq (16) is recalled, in the form of

$$\left(\frac{\partial^2}{\partial x^2} + \frac{\partial^2}{\partial y^2} + \frac{\partial^2}{\partial z^2}\right)\vec{E}_1 + \mu\varepsilon\omega^2\vec{E}_1 = \mu\frac{\partial^2 \vec{P}_{NL}}{\partial t^2} \tag{36}$$

If waves are assumed traveling in the z direction, z>>x,y ,of

$$E_1(r_\perp, z) = \mathcal{E}_1(r_\perp, z) e^{ikz} \tag{37}$$

and

$$\frac{\partial^2}{\partial x^2} + \frac{\partial^2}{\partial y^2} = \nabla_t^2 \tag{38}$$

then, when $\frac{\partial^2 \mathcal{E}}{\partial z^2}$ is ignored as very small,

$$\frac{\partial \mathcal{E}_1}{\partial z} - \frac{i}{2k_1}\nabla_t^2 \mathcal{E}_1 + \frac{i\mu}{2k_1}\frac{\partial^2 P_{NL}}{\partial t^2} = 0 \tag{39}$$

If a solution such as eq (34) is chosen for the driving term causing the P_{NL} , then eq (39) may be rewritten as

$$\frac{\partial \mathcal{E}_1}{\partial z} - \frac{1}{2ik_1}\nabla_t^2 \mathcal{E}_1 + \frac{g^2(r_\perp, z)}{2}\mathcal{E}_1 = 0 \tag{40}$$

g is the afore mentioned gain without the loss terms α and α_s. g is related to the pump field by some constant A

$$g^2(r_\perp, z) = A\,|E_2(r_\perp, z)|^2 \tag{41}$$

Neglecting depletion and loss, the pump E_2(ommiting the time dependence now)

$$E_2(r_\perp, z) = \mathcal{E}_{p2}(r_\perp, z)\, e^{-ikz} \tag{42}$$

obeys

$$\frac{\partial \mathcal{E}_{p2}}{\partial z} - \frac{1}{2ik_2}\nabla_t^2 \mathcal{E}_{p2} = 0 \tag{43}$$

Now a system of functions may be constructed such that

$$\frac{\partial f_k}{\partial z} - \frac{1}{2ik}\nabla_t^2 f_k = 0 \tag{44}$$

where f_k are orthogonal, according to

$$\int f_n^*(r_\perp, z)\, f_k(r_\perp, z)\, dr_\perp = \delta_{nk} \tag{45}$$

f_0^* is chosen so that it is related to the incident pump field through some constant B

$$\mathcal{E}_{p2}(r_\perp, z) = B f_0^*(r_\perp, z) \tag{46}$$

The scattered field can be expanded in a linear combination of these orthogonal functions

$$\mathcal{E}_1(r_\perp, z) = \sum_{k=0}^{\infty} C_k(z)\, f_k(r_\perp, z) \tag{47}$$

Replacing all the defined values for $\mathcal{E}_1$, g, and $\mathcal{E}_2$ into eq (44) one derives

$$\sum_{k=0}^{\infty} C_k \frac{\partial f_k}{\partial z} + f_k \frac{\partial C_k}{\partial z} - \frac{i}{2k} C_k \nabla_\perp^2 f_k(r_\perp, z) + \frac{1}{2} AB^2 |f_0|^2 C_k f_k = 0 \tag{48}$$

The center two terms on the left are zero, as defined in (44). Multiplying through by

$$\int dr_\perp f_i^*(r_\perp, z) \tag{49}$$

produces

$$\frac{dC_i}{dz} + \frac{1}{2} \sum_{k=0}^{\infty} g_{ik}(z) C_k(z) = 0 \tag{50}$$

where

$$g_{ik}(z) = AB^2 \int |f_0|^2 f_i^* f_k \, dr_\perp \tag{51}$$

This states that, if $|f_0|^2$ fluctuates strongly in $r_\perp$, only the term g_{00} will be of appreciable magnitude, since

$$g_{00}(z) = AB^2 \int |f_0|^4 dr_\perp \tag{52}$$

Thus C_0 grows the most quickly and dominates. Finally

$$\begin{aligned} \mathcal{E}_1(r_\perp, z) &= \sum_{k=0}^{\infty} C_k(z) f_k(r_\perp, z) \simeq C_0 f_0 \\ &= -\frac{C_0(z)}{B^*} \mathcal{E}_2^*(z) \end{aligned} \tag{53}$$

and the scattered field is conjugate to the incident field.

Transverse Modes.

Frieberg and Drummond (5:5618) have theoretically considered a

configuration in which a dielectric partial reflector precedes a phase conjugate mirror (PCM). The system consists of free space, a lossless dielectric mirror of index $n>1$, and a phase conjugate mirror (see Figure 3). It was assumed that no frequency shift occurred upon PCM reflection.

The waves involved are of the form

$$\vec{E}_j(\vec{r}) = \epsilon_j A_j e^{i\vec{k}\cdot\vec{r}} \tag{54}$$

where ϵ_j is the real polarization vector, $\vec{k}_j$ is the wave vector, and A_j is the complex electric field amplitude of the jth wave. For the case in which the amplitude reflection coefficient of the mirror and the PCM are r and μ respectively (and are in general complex)

$$A_2 = r\frac{(1-|\mu|^2)}{(1-|r|^2|\mu|^2)} A_1 \tag{55}$$

and

$$A_5 = \mu\frac{(1-|r|^2)}{(1-|r|^2|\mu|^2)} A_1^* \tag{56}$$

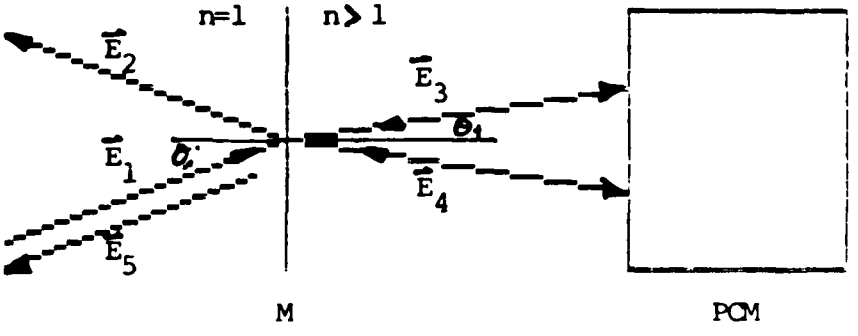

Figure 3 Specular reflection cancellation in a dielectric and phase conjugate mirror configuration (5:5621)

where A_2 and A_5 are the complex electric field amplitudes of the specular and phase conjugate reflections respectively.

In the limiting cases the properties of eqs (55) and (56) are apparent. With $|\mu| \to 0$ there is the trivial case of

$$A_2 \to r A_1 \tag{57}$$

and

$$A_5 \to 0 \tag{58}$$

With $|\mu| \to 1$

$$A_2 \to 0 \tag{59}$$

and

$$A_5 \to e^{i\phi} A_1^* \tag{60}$$

where ϕ is the phase of μ .

Eqs (59) and (60) state that when the PCM reflectivity is 100% the mirror specular reflection is cancelled and the total field outside the dielectric is

$$\vec{E}(\vec{r}) = \vec{E}_1(\vec{r}) + e^{i\phi}\vec{E}_1^*(\vec{r}) \tag{61}$$

Eqs (55) and (56) dictate the response of the mirror system for different values of r and μ , but in general the PCM drives the reflection results more as r gets smaller and μ gets larger.

Again, the above argument is based on not having a frequency shift upon PCM reflection. In the case of SBS there is a finite shift, and this changes things considerably, even if 100% SBS reflectivity is achieved. The SBS cell is necessarily separated from the partially reflecting output coupler in the experimental setup being considered. In this case the separation is 26.05 cm. The SBS shift corresponds to

.015 nm at the Nd:YAG wavelength and there are about 3.45 more wavelengths of the incident λ_i in this distance than the reflected and shifted wavelength λ_r .

If the SBS took place in an infinitly small region the distance between the SBS cell and the output coupler could be adjusted so that the two wavelengths were 'in phase' at the output coupler. The interference that causes A_2 to go to 0 might still occur to some extent. In the case of a waveguide tube, however, there may be several interaction regions displaced over a large distance. In addition the multimode nature of the beam produces a corresponding multi-region SBS interaction. The above argument for $A_3 \rightarrow 0$ cannot hold in this case.

The effects of the output coupler cannot be ignored then, and the transverse mode properties of the PCR must be examined with consideration of the boundary conditions that the output coupler imposes. Auyeung et al. (1:1180) have considered the transverse mode properties of a PCR with a conventional mirror and a PCM employing degenerate four wave mixing (DFWM).

For a PCR using DFWM, the self consistency field requirement may be met by one and two round trip field solutions (see Figure 4). For the degenerate case (no frequency shift) and one round trip field consistency there is no constraint on the Gaussian spot size, while the radius of curvature must match that of the conventional mirror. For two round trip (TRT) consistency there are no restrictions on the radius of curvature or spot size of the Gaussian beam. Any complex radius of curvature,

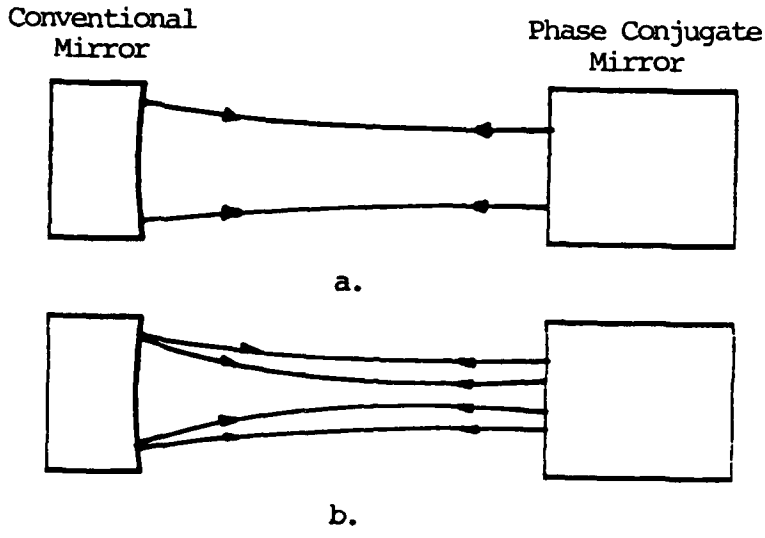

Figure 4 Self consistent field solutions for a PCR. a) one round trip, b) two round trips

$$\frac{1}{q} = \frac{1}{R} - \frac{\lambda}{\pi w^2} \tag{62}$$

where R is the radius of curvature and w the spot size, will be self consistent for the TRT degenerate case.

For the nondegenerate DFWM case the incident field is at frequency $\omega+\delta$ and the reflected field is at $\omega-\delta$. This argument works as well for the case of SBS if the SBS shift $\Delta\omega_{SBS} = 2\delta$, except in the SBS case the incident spot size w_i is larger than the reflected spot size w_r due to the SBS process threshold (for the DFWM case w_i can equal w_r) (7:3719). The result for the complex radius of curvature is, for SBS,

$$q_r = -q_i^* \left(1 - \frac{\Delta\omega_{SBS}}{\omega}\right) \tag{63}$$

Also upon SBS reflection

$$\lambda_r = \lambda_i + \Delta\lambda_{SBS}$$
$$w_r < w_i \qquad (64)$$
$$R_r = R_i$$

The reflected Gaussian beam has properties, therefore, that distinguish it from the incident beam.

These results can now be considered with respect to the three mirror configuration employed for this thesis. The startup resonator, shown in a simplified form in Figure 5, has but one self consistent solution. This transverse mode must have a very large radius of curvature at the mirrors, given that the experimental cavity was of flat-flat mirror configuration. If this mode is assumed to be TEMoo for simplicity (it certainly was not the case in reality) this cavity would have, at some position, a waist w_o . The position of this waist cannot be practically stated due to the cavity stability. From the waist position, wherever that may be, the equations governing Gaussian beam propogation could be used to find the spot size and radius of curvature at all points. For a given spot size and radius of curvature the equation for the distance to the beam waist is

$$z = \frac{R}{1 + \left(\frac{\lambda R}{\pi w^2}\right)^2} \qquad (65)$$

and the waist size is

$$w_o = \frac{w}{\left[1 + \left(\frac{\pi w^2}{\lambda R}\right)^2\right]^{1/2}} \qquad (66)$$

If the spot size aperturing effect of the SBS threshold is assumed to be .8 w_i, a conservative estimate for the low reflectivities encountered in this experiment, the equation for the distance to the

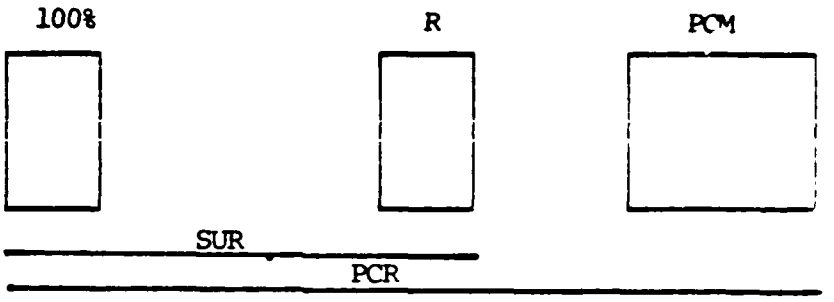

Figure 5 Simplified three mirror PCR configuration. The startup resonator (SUR) and phase conjugate resonator (PCR) are designated.

waist is, given an incident spot size and radius of curvature of w_i and R_i respectively and a reflected spot size of $w_r = .8 w_i$,

$$z = \frac{R_i}{1 + 2.44\left(\frac{\lambda R_i}{\pi w_i^2}\right)^2} \tag{67}$$

(The wavelength shift is negligible and $\lambda_i \simeq \lambda_r$.) Thus, upon reflection the distance to the waist has been altered. In this case the parenthetical denominator term is of order 1 (assuming w_i = 2mm, R_i=10m, and λ =1.06μm , the term is about .7). It can be seen that the result of the reduced reflected spot size, while maintaining the same radius of curvature as the incident beam, is that the beam waist position is translated by a substantial amount.

The same argument can be put forth for the waist spot size associated with the reflected beam, in terms of the incident beam parameters and $w_r = .8 w_i$,

$$w_0 = \frac{.8 w_A}{\left[1 + .4096 \left(\frac{\pi w_A^2}{\lambda R_A}\right)^2\right]^{1/2}} \qquad (68)$$

In this case the net effect of SBS reflection is the reduction of the waist size by nearly the aperturing factor.

Because of the change in position and size of the waist upon SBS reflection it appears that one round trip self consistency cannot be achieved. Two round trip self consistency is disallowed, it appears, by the necessity to match the boundary conditions imposed by the output coupler. Therefore the transverse mode properties associated with the PCR are complicated and transient in nature.

Spectral Control.

In order to produce high reflectivities from SBS it is necessary to provide a narrow-linewidth startup resonator. Because of the strong tendency for a Nd:YAG laser to operate with relatively broad spectral characteristics (the gain linewidth is about 6 cm^{-1}) measures must be taken to narrow the linewidth of the SUR. The approach taken was the introduction of various etalon elements, including resonant reflectors, to the SUR.

The spectral response of the four different elements are shown in Figure 6. They are, in order, a six element resonant reflector, a one element resonant reflector, a Korad etalon, and a two element etalon. The Figure includes the linewidth measured for a particular cavity with a relatively high threshold (the cavity consisted of: a 27% output coupler, no etalon elements, no apertures, flat-flat mirror configuration), and the primary 1.06 μm wavelength and the first two

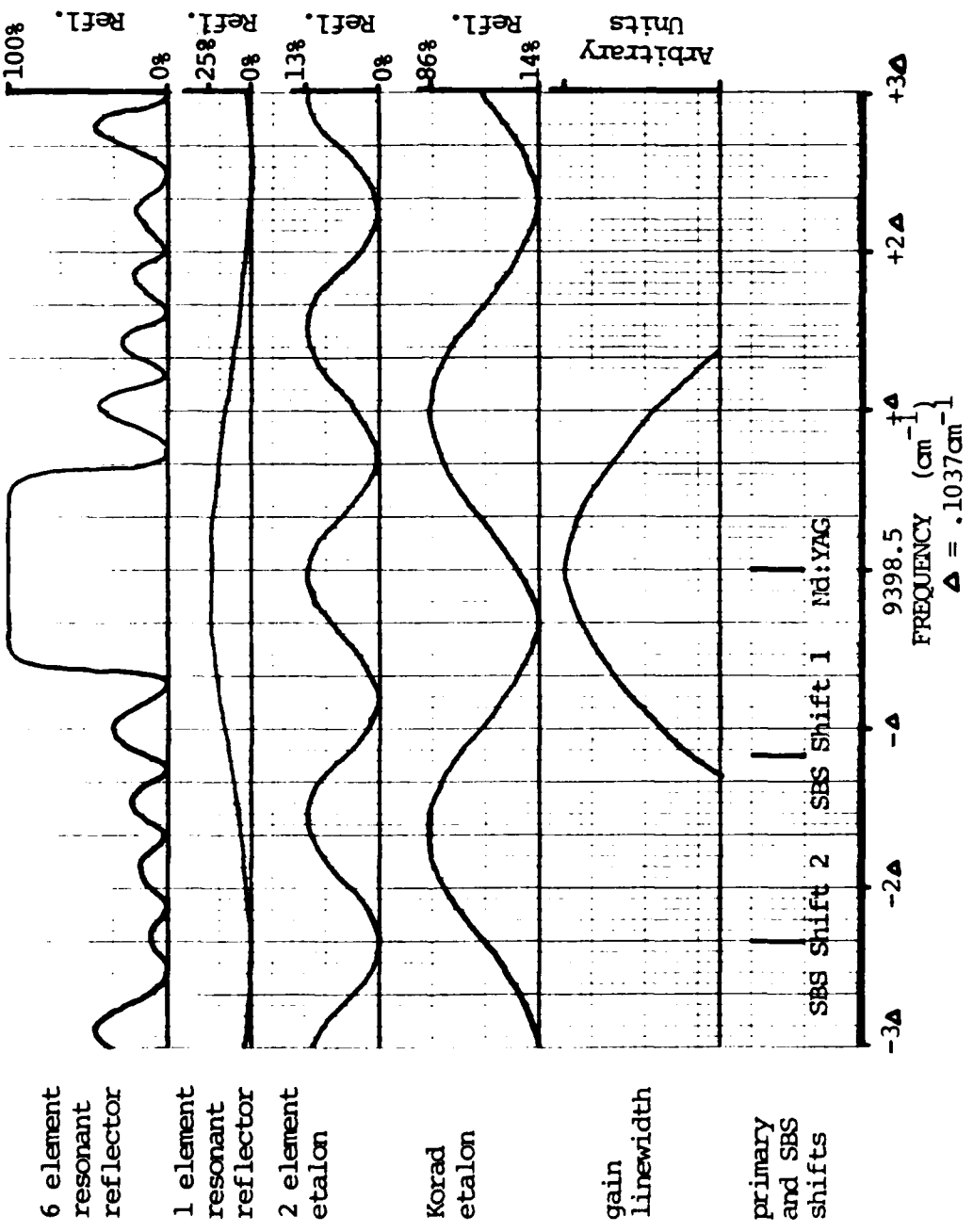

Figure 6 Spectral response of various etalon elements

SBS shifted wavelengths.

The resonant reflectors are a product of Laser Optics Inc., and are called 'Ekalons'. They consist of specially treated uncoated glass elements, with an index of 1.74. The high index affords high reflectivity without having to resort to sapphire and its inherent problems and cost. The spectral response used in Figure 6 was drawn from that provided by Laser Optics Inc with the devices.

The Korad etalon was 12.5 mm thick and had 45% reflective coatings. The response of this device was found using the appropriate equations, and the curves shown are an approximation of the nearly sinusoidal spectral response.

The two element etalon was constructed from optical flats, and the response shown in Figure 6 is a best case condition for reflectivity. The alignment of the device could be such that the reflectivity was minimal, falling into a null region of the spectral response envelope dictated by the smallest element dimension.

The four devices described were placed in the cavity in various combinations. The resonant reflectors were aligned for peak laser performance, and hence had their peak reflectance tuned to the peak of the gain curve. The other two devices were placed in the cavity at some small angle, and hence the actual position of the spectral response curves with respect to the gain curve was not known. Their curves shown in Figure 6 are positioned arbitrarily.

Because the SBS reflectivity is strongly dependent on the linewidth of the SUR, the net spectral response of the cavity greatly influences the PCR performance. The absolute and relative positions of the

spectral responses of the elements placed in the cavity was not known, and it is highly likely that the responses drifted relative to one another because of thermal wander. In order to control the cavity spectral response the etalon elements would have to be temperature controlled, and that was not possible in this experiment.

III. PCR Setup and Diagnostic Equipment.

The actual experimental setup employed for the PCR is described in this section, along with the approach and methodology used in its construction, alignment, and operation. A description of the diagnostic equipment is also presented.

Cavity Dumped Startup Resonator.

In order to initiate SBS a threshold fluence must be introduced in the nonlinear material that will be employed. This threshold is a function of several parameters (wavelength, spectral linewidth, pulse duration, spot size, interaction length), but it is clear that there must already be a laser oscillator to produce a PCR. In this thesis a Nd:YAG oscillator collinear and interior to the PCR was used as the startup resonator (see Figure 1). The SUR was operated in a Q-switched cavity dumped mode. This provided the SBS cell with the fluence necessary for operation, through the output coupler, and also the means to output energy from the PCR (cavity dump). The SUR could also be operated in the cavity dump mode without the SBS cell. The SUR consisted of, in linear order:

a. A high reflector; this was either curved or flat, and was later replaced with a resonant reflector (to be discussed).

b. An etalon; 45% reflectance, 12.5 mm thick, sometimes not employed.

c. An electro-optic element; the cavity dump switch, operated AC coupled (normally at 0 voltage).

d. A polarizing element; a Glan-air polarizer.

e. The laser head; consisting of a .25X3 inch Nd:YAG laser rod and a single Xenon flashlamp in a diffuse circular cylinder pump cavity.

f. A polarizing element; another Glan-air polarizer.

g. An adjustable aperture; an iris.

h. An electro-optic element; the Q-switch, operated DC coupled (normally at quarter wave voltage).

i. An output coupler; of various reflectances, sometimes replaced with a resonant reflector.

Alignment of the SUR.

The SUR alignment process began, using an alignment HeNe laser, with the Nd:YAG laser rod. All optical elements were aligned to the laser rod, starting with the farthest elements from the HeNe laser. The retro-reflection technique was used. The initial SUR employed a positive 10 meter radius of curvature high reflector and 99% reflectance flat 'output coupler'; the threshold for laser oscillation was very low. All elements were aligned for minimum lasing threshold in long pulse lasing mode. The Glan-air polarizers were aligned for intracavity polarization in the plane of Figure 1, and thus the electro-optic cavity dump produced an output polarization perpendicular to the plane of Figure 1. The polarizer adjacent to the cavity dump switch was used as the output coupling optic.

The electro-optical elements were optimized for their quarter wave voltage and alignment. The alignment is not, in general, optimal for the case of retro-reflection alignment. Each of the cavity dump (CD)

and Q-switch (QS) elements were optimized in turn, while the other element remained passive. For alignment each element was DC coupled and untriggered. The voltage to the element was adjusted for a given input energy to the laser head so as to minimize long pulse laser oscillation. Once laser oscillation had been suppressed the energy to the head was increased and the element voltage again adjusted to hold off lasing. Once this process had been completed the orientation of the element was adjusted, again to maximize hold-off of laser oscillation. It was found that the orientation of the elements was considerably away from that position determined by HeNe retroreflection.

The QS driver was triggered, after a 220 us delay, from a 'fire' pulse generated by the laser pulse forming network (PFN) upon initiation of the discharge of the capacitor bank. The QS driver was an Inrad Model 2-016. It lacked a fast enough rise time to be used as a CD driver, but had a very stable firing circuit.

The CD driver was initially triggered from the QS driver 'trigger out' through an HP1310 pulse generator so as to allow a variable delay between QS and CD switching. The HP delay generator was found to have considerable jitter, so finally the CD driver was connected directly to the QS driver 'trigger out'. Although the QS to CD delay could have been adjusted by varying the length of the coax cable between their triggering circuits (1.47 ns/ft for RG58 coax) the SUR operated optimally for a minimum cable length. The initial driver employed, an Inrad Model 2-015, was replaced after it failed by a Lasermetrics Model GP4. Both units had very fast rise times. The cavity dump element was AC coupled so that a quarter wave plate was not necessary for operation.

SBS Medium.

The SBS medium, as stated before, was carbon disulfide (CS_2). This liquid was chosen because of its advantageous characteristics as a nonlinear material. It has high gain, low threshold, and forgiving spectral properties. It does have several drawbacks. It has a high vapor pressure and low flash point. It is highly toxic. Handling practices had to be stringently cautious.

In practice the CS_2 was only open to the atmosphere under a Class III fume hood. Goggles, mask, and gloves were required whenever the material was handled. This turned out to be fairly frequent because CS_2 degraded with use. The degradation could be minimized by minimizing the exposure of the CS_2 to room light, and by minimizing breakdown of the CS_2 by too high a laser flux density.

Figure 7 SBS cells. Top is cylinder tube and bottom is waveguide tube

An annoying property of the CS_2 is its high expansivity. The laboratory could sometimes get fairly warm during an experiment, and this led to the expansion of the CS_2. If not enough room had been left in the SBS cell for the expansion, CS_2 overflow could occur.

Two SBS cells were investigated (see Figure 7), both constructed of Pyrex. The first, a cylinderical tube, did not perform well at the onset, and it was not used again. The second cell, and the cell on which all data were taken, consisted of a waveguide tube enclosed in an outer shell. The windows had a flatness of $\lambda/20$ before they were heated for construction (see Figure 8).

It was found that the optimum direction for waveguide alignment was collinear to the SUR. This was an undesirable configuration for the sake of diagnostics; the reflection off of the window could confuse

Figure 8 Front view window of waveguide SBS cell

determining if phase conjugation was occurring. It was impossible to obtain in any case due to damage to the cell window, on both ends, at the onset of investigations. This damage was peculiar in that it occurred on the inside of the windows in all cases (there were several cases of cell window damage).

Diagnostics.

A variety of diagnostic tools were used to observe the PCR performance. These included monitors for pulse shape, energy, spectral content, and transverse mode characteristics. The equipment and method of employment will here be discussed.

Pulse Shape.

The output of the lasers (SUR and PCR) were monitored in time by Quantum Electronics Series AD210 high-speed amplified photodiodes. The devices had a rise time of less than 250 ps, and a FWHM less than 500 ps. The detectors were placed to view: 1. The cavity dumped output of the laser (SUR or PCR), 2. The SBS reflection from the CS_2 cell, and 3. The signal through the waveguide tube. Each device was protected from over irradiation by expanding the beams onto a lambertian scatterer, and placing the required number of neutral density filters in front of the detector. Over irradiation of the devices resulted in saturation of the detector amplifiers, and a large increase in the fall time of the signal. The output of the detectors was viewed on Tektronics Model 7633 storage oscilliscopes.

Pulse Energy.

Pulse energy measurements were taken using Photodyne Model 66XLA

Optical Power/Energy Meters using the Model 350 Sensor Head. The Sensor Head was esentially a miniature integrating sphere. Three of these meters were used, monitoring: 1. The cavity dump output (SUR or PCR), 2. The energy incident upon the cell window, 3. The energy reflected from the cell. Each device was calibrated in place using a Scientech Energy/Power Meter and head. (The Scientech was used exclusively for calibration.) Once a scale factor had been determined for each device (they varied considerably) via calibration, energy values could be derived from the Photodyne readings.

Spectral Content.

The spectral output of the laser was monitored using a Gaertner Fabry-Perot interferometer with a 1 cm gap and silver mirrors (see Figure 9). The output of the laser was incident upon the interferometer through a -20 cm lens, and the ring pattern was focused, after being redirected, on a

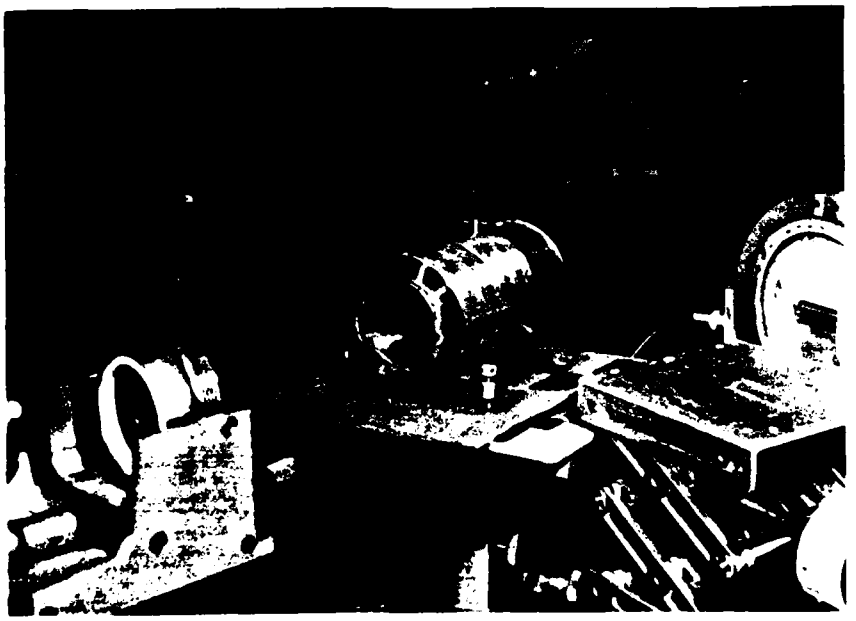

Figure 9 Fabry-Perot setup

1000 element linear array. The array output, a linear cross-section of the ring pattern, was displayed on a Tektronics oscilliscope.

Transverse Mode Pattern.

The output spot image was viewed by an image analysis system from Interpretation Systems Incorporated (ISI), using the storage capacity of a Colorado Video Frame Grabber. A diagram of the system is shown in Figure 10. The system included, from laser spot to display:

1. A Cohu Inc. Television Camera: focused on a lambertian surface with a microscope objective.
2. A Cohu Inc. Television Camera Control Unit.
3. A Colorado Video Inc. Frame Grabber.

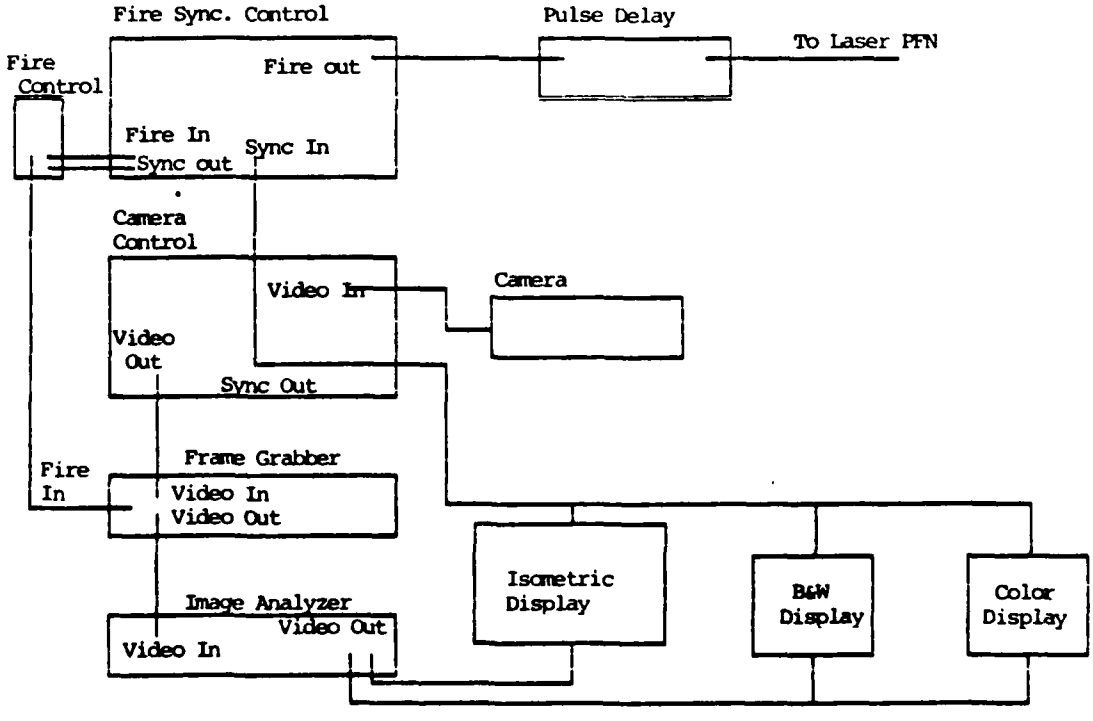

Figure 10 Diagram of image analysis system

the laser at the same PFN voltage virtually impossible. The charging cycle was signalled to the operator by an audible 'click', whereupon the maximum voltage was present at the capacitors. The fluctuation of the PFN voltage was about 15 volts throughout the PFN range, or about 2 J fluctuation in the energy supplied to the lamp. This was intolerable, so that the laser was manually fired as soon after the charging cycle 'click' as was physically possible. The percentage fluctuation in the energy supplied to the lamps was drastically reduced by this method, since the charging cycle ranged from 3 to 5 seconds throughout the operating range.

IV. Experimental Results.

This section will present the results of the PCR performance, primarily in the form of energy in (into the lamps) versus energy out (cavity dumped energy) curves. Spot images and spectral content will also be displayed. The performance of the SUR without SBS or any etalon elements will be dealt with first, and then the results for the PCR optimization and subsequent aberration.

SUR Performance.

Data was taken for the SUR with a bare cavity, i.e. no etalon or aperture elements. The results for 100%, 45%, 35%, and 27% output couplers are shown in Figure 11. (All lines on the following graphs are 'guides to the eye' .) The curve for the 100% output coupler is, of course, the optimum to be expected from a cavity dumped laser with conventional mirrors. The associated spot images for different output couplers are shown in Figures 12 (100%) and 13 (27%). As output coupler reflectivity was reduced the spot quality suffered. As expected, the pulse width got larger with lesser output coupler reflectivity, going from 20ns for 100% output coupler to 35ns for 27% output coupler.

The addition of a 100% mirror outside the partial reflecting output couplers was also investigated. The results are shown in Figure 14 along with the results for a 100% output coupler alone. The double mirror configurations cavity dump energy output performance fell very nearly upon each other. The loss associated with these double mirrors did effect the performance with respect to the single 100% mirror case, as expected. The pulse width of 40ns was the same for all cases.

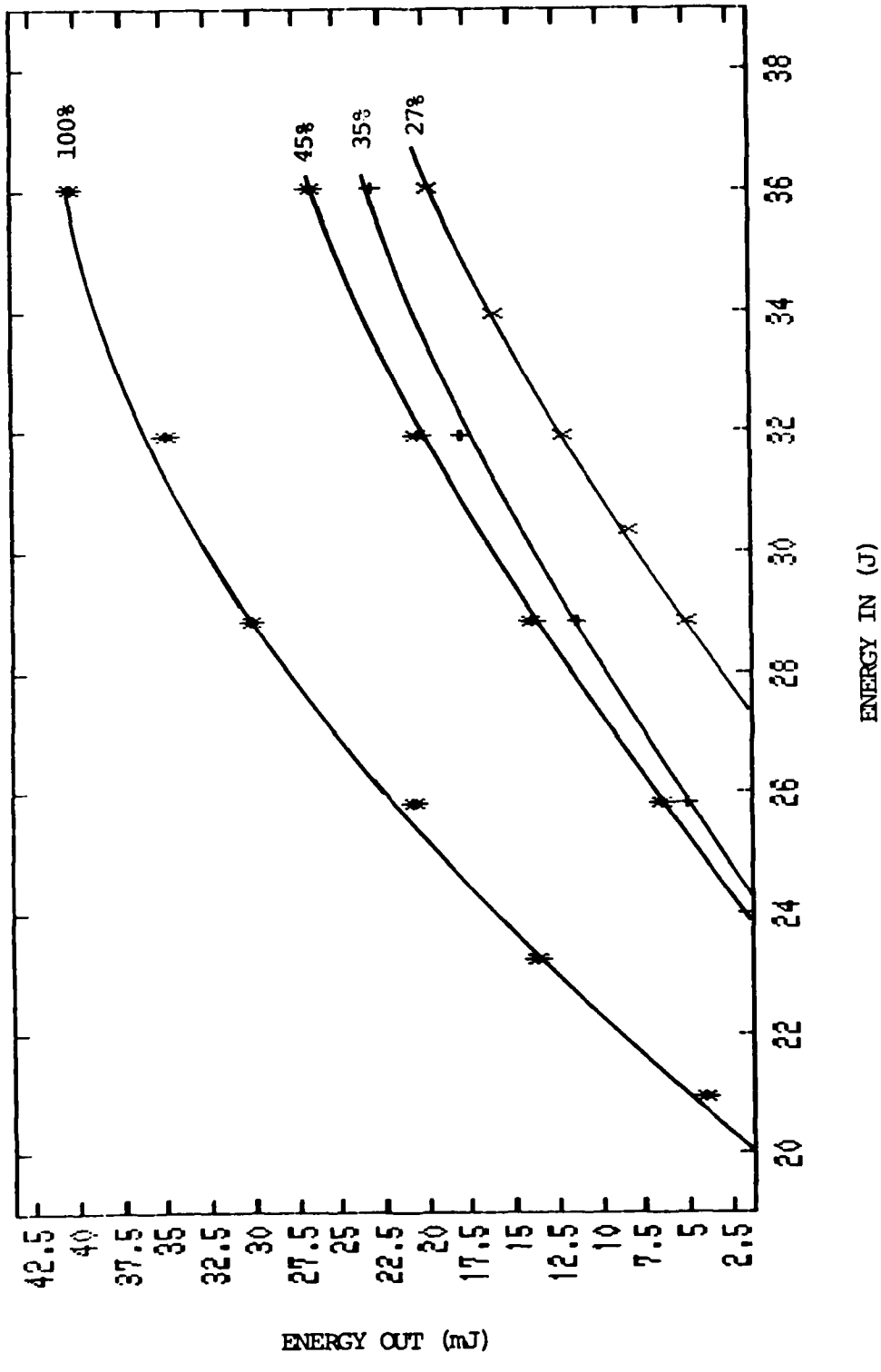

Figure 11 Graph of SUR results for 100%, 45%, 35%, and 27% output couplers. '*'-100%, '*'-45%, '+'-35%, 'x'-27%

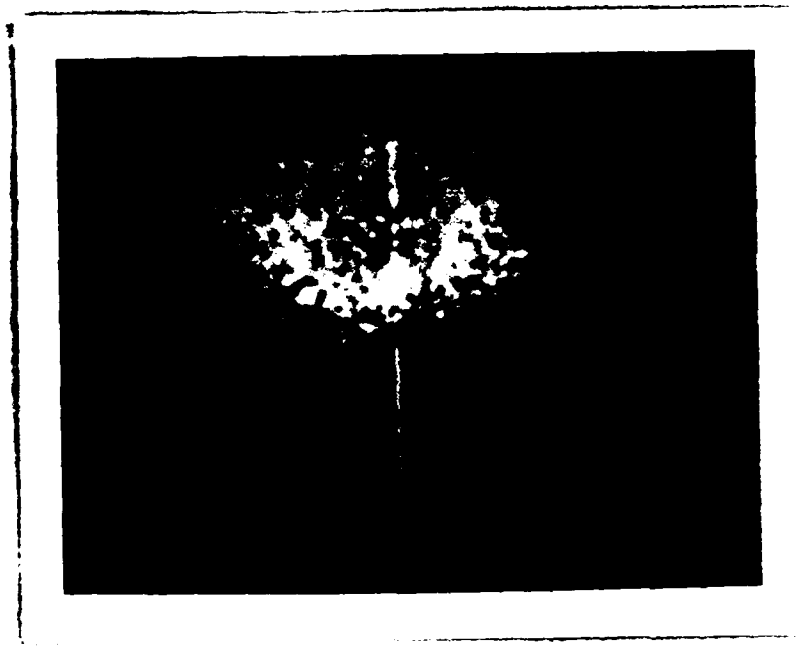

Figure 12 Spot image for SUR with 100% output coupler

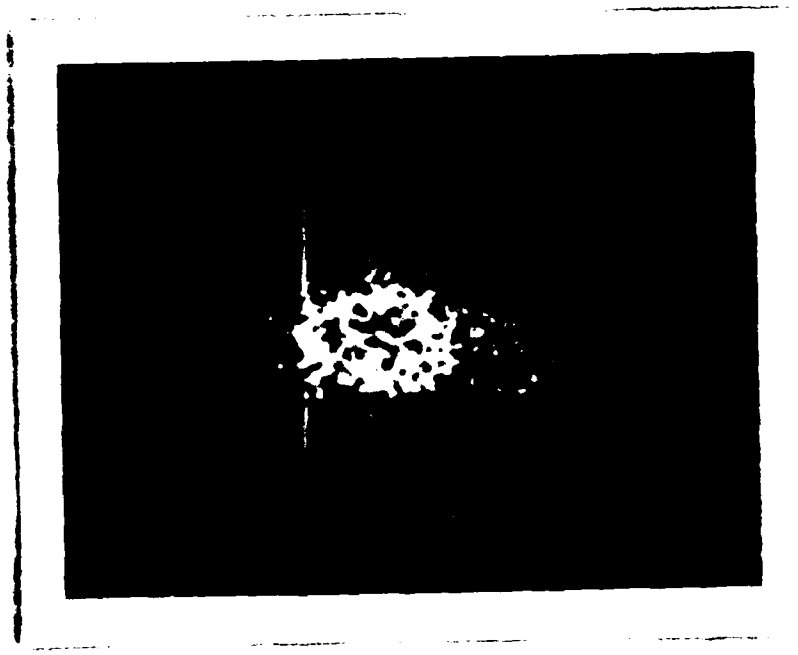

Figure 13 Spot image for SUR with 27% output coupler

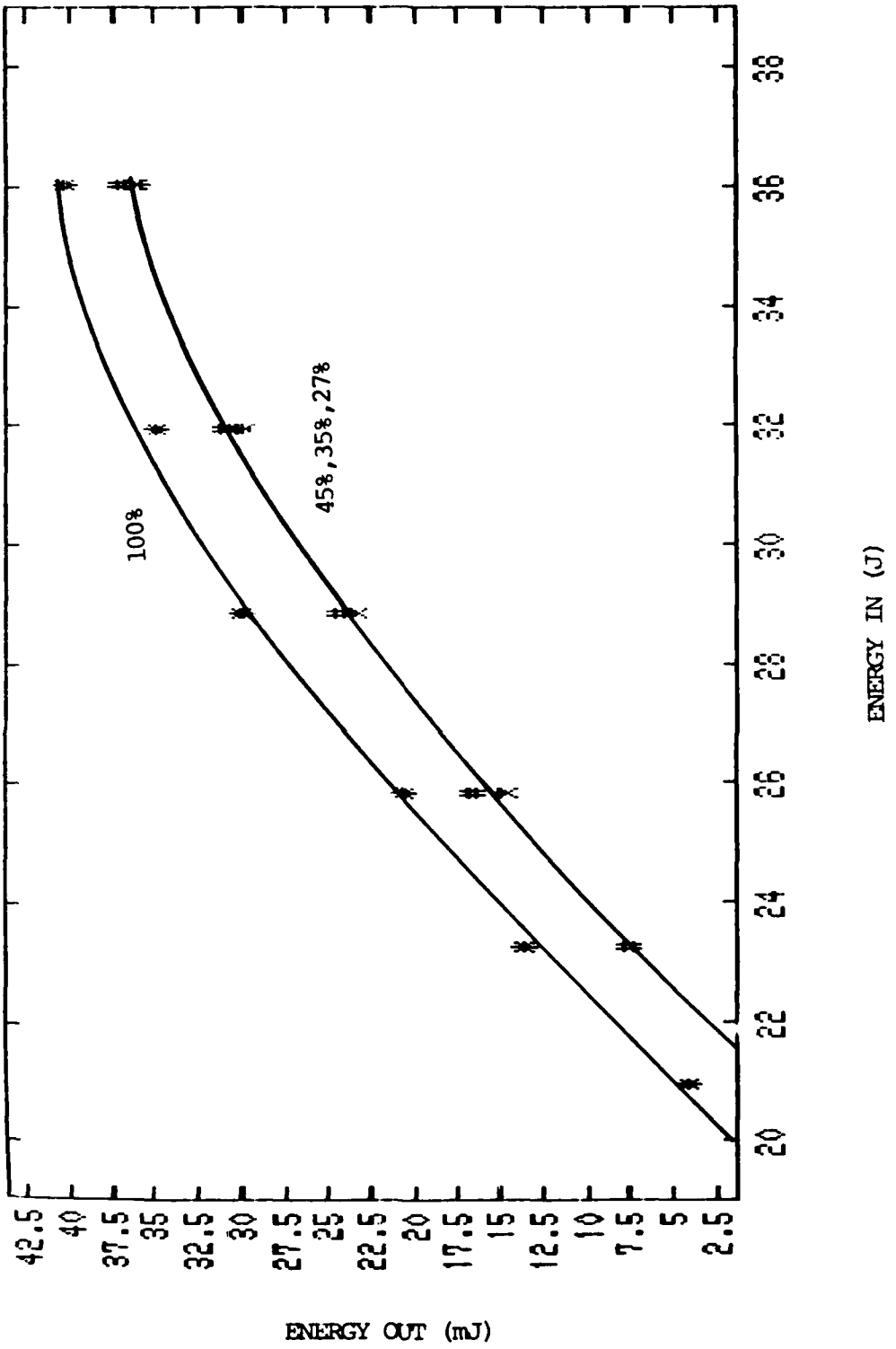

Figure 14 Three conventional mirror setup results; for 45%-'*', 35%-'+', and 27%-'x', with results for 100% alone-'*'

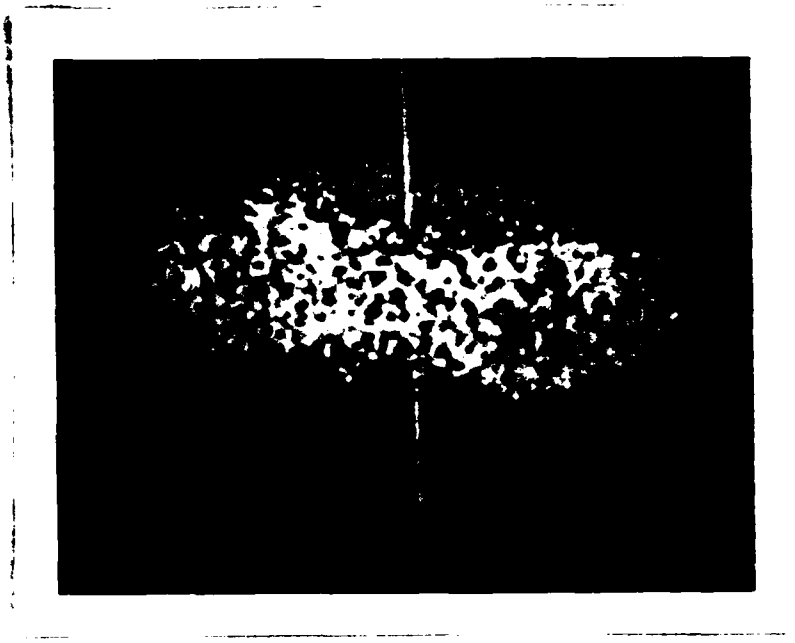

Figure 15 Spot image for 27% output coupler

The addition of the third mirror, however, had a detrimental effect on the quality of the spot image (Figure 15 is the spot image for the 27% output coupler case). This is not surprising considering the alignment tolerance that must be kept between the three mirrors (high reflector, partial reflecting output coupler, and 100% third mirror) and the rich interaction that these elements had with all the other less than ideal elements present in the cavity.

PCR Performance.

Unapertured and Aligned.

The first successful attempt at a PCR employed a 27% output coupler and a Korad etalon. Previously, a cavity with no line narrowing elements had failed to produce a PCR. The improvement to cavity dump energy output was low due to the low SBS reflectivity (see Figure 16).

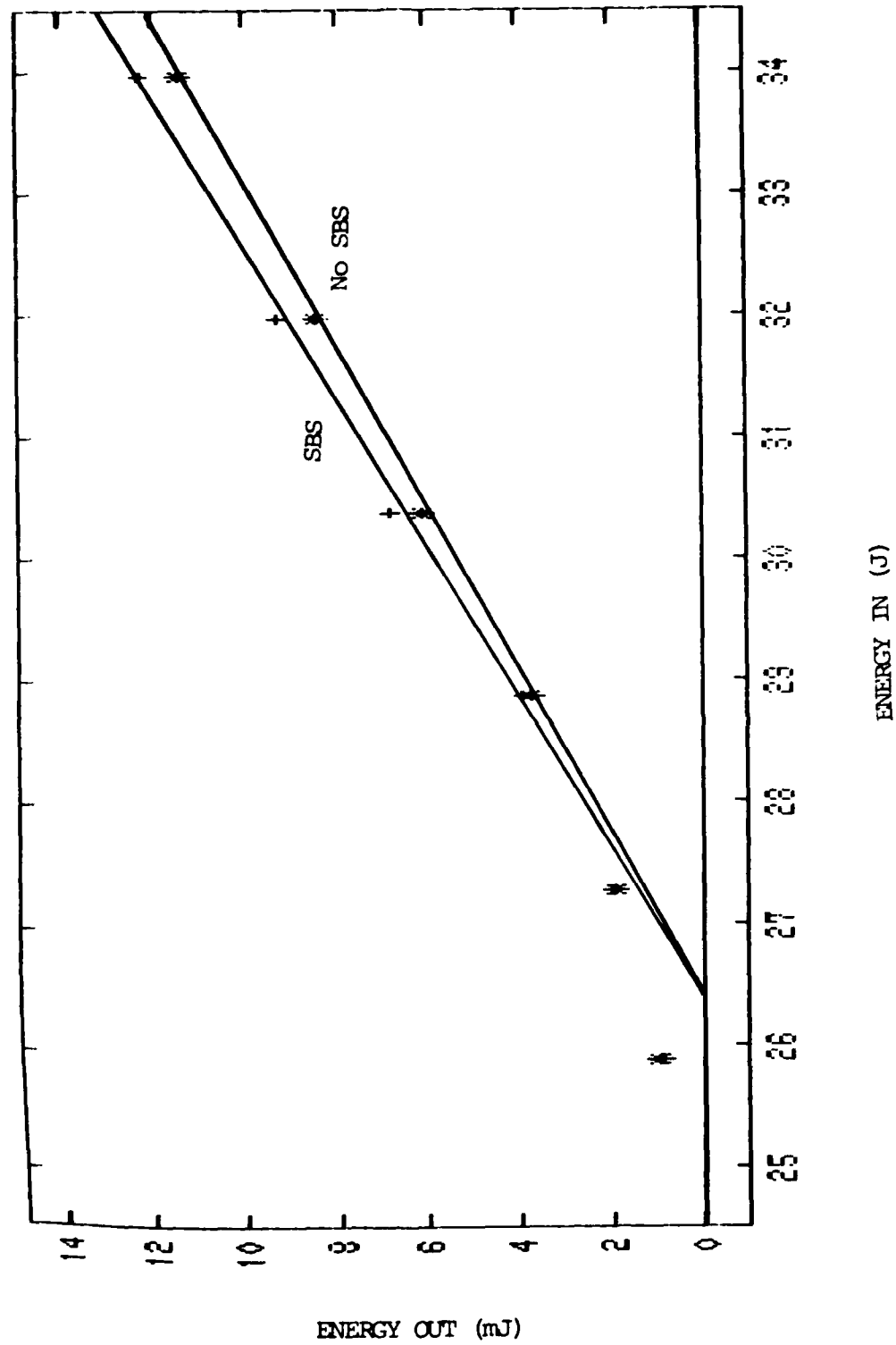

Figure 16 PCR performance for 27% output coupler and Korad etalon
'*'-no SBS, '+'-with SBS

This was due to the large linewidth characteristic of the SUR.

To reduce the linewidth of the SUR, a double-element etalon was fabricated from two uncoated optical flats. This element was placed in the cavity between the Q-switch and the output coupler. The Korad etalon remained in the cavity. The energy performance of the PCR did improve somewhat (see Figure 17) compared to that of just the Korad etalon present, but still was less then impressive.

The double element etalon was removed, and the 27% output coupler was replaced with a one element resonant reflector. Again the Korad etalon was left in the cavity. These results are shown in Figure 18. In this case the improvement to cavity dumped energy was more pronouced. With the Fabry-Perot interferometer it was possible to observe the spectral properties of the output. The traces, with and without SBS, are shown in Figures 19 and 20 . The $.12cm^{-1}$ shift calculated from the data, corresponds very well with the theoretical value of $.126cm^{-1}$ given in the literature (20:603).

The shift seen in Figure 20 is, at first glance, toward shorter wavelengths. The feature, however, belongs to the order m-1 if the large peak on the left of the traces is assumed to be order m. The spacing between adjacent orders for the shifted feature (marked 'B' in Figure 20) is seen to be larger (this will be more obvious in traces to be shown later) than the spacing for the unshifted, larger, peaks (marked 'A' in Figure 20). From this spacing data the shift amount was calculated.

The maximum performance obtained occurred when the high reflector was replaced by a 6 element resonant reflector, and the Korad etalon was

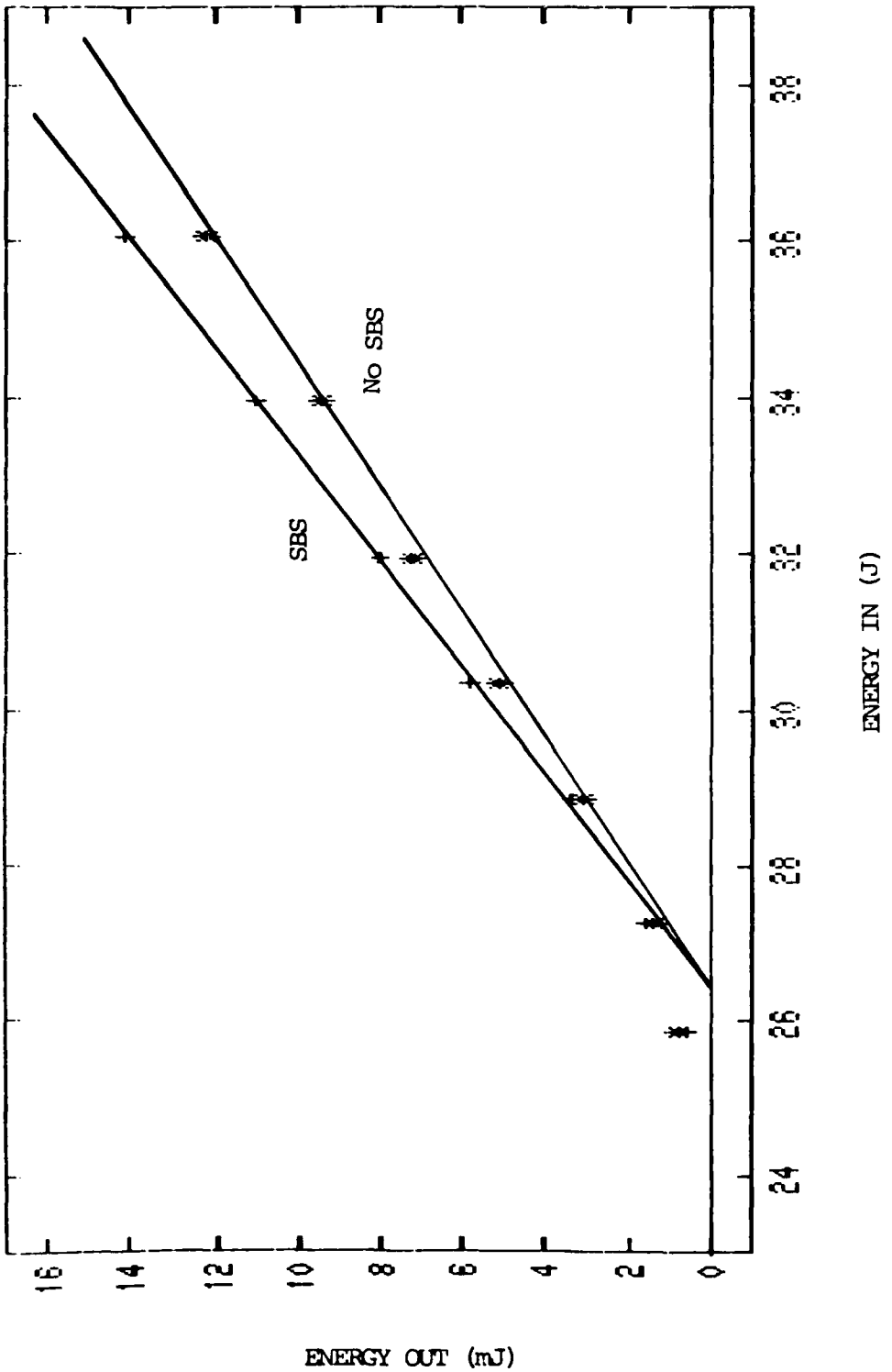

Figure 17 PCR performance with Korad and two element etalons.
'*'-no SBS, '+'-with SBS

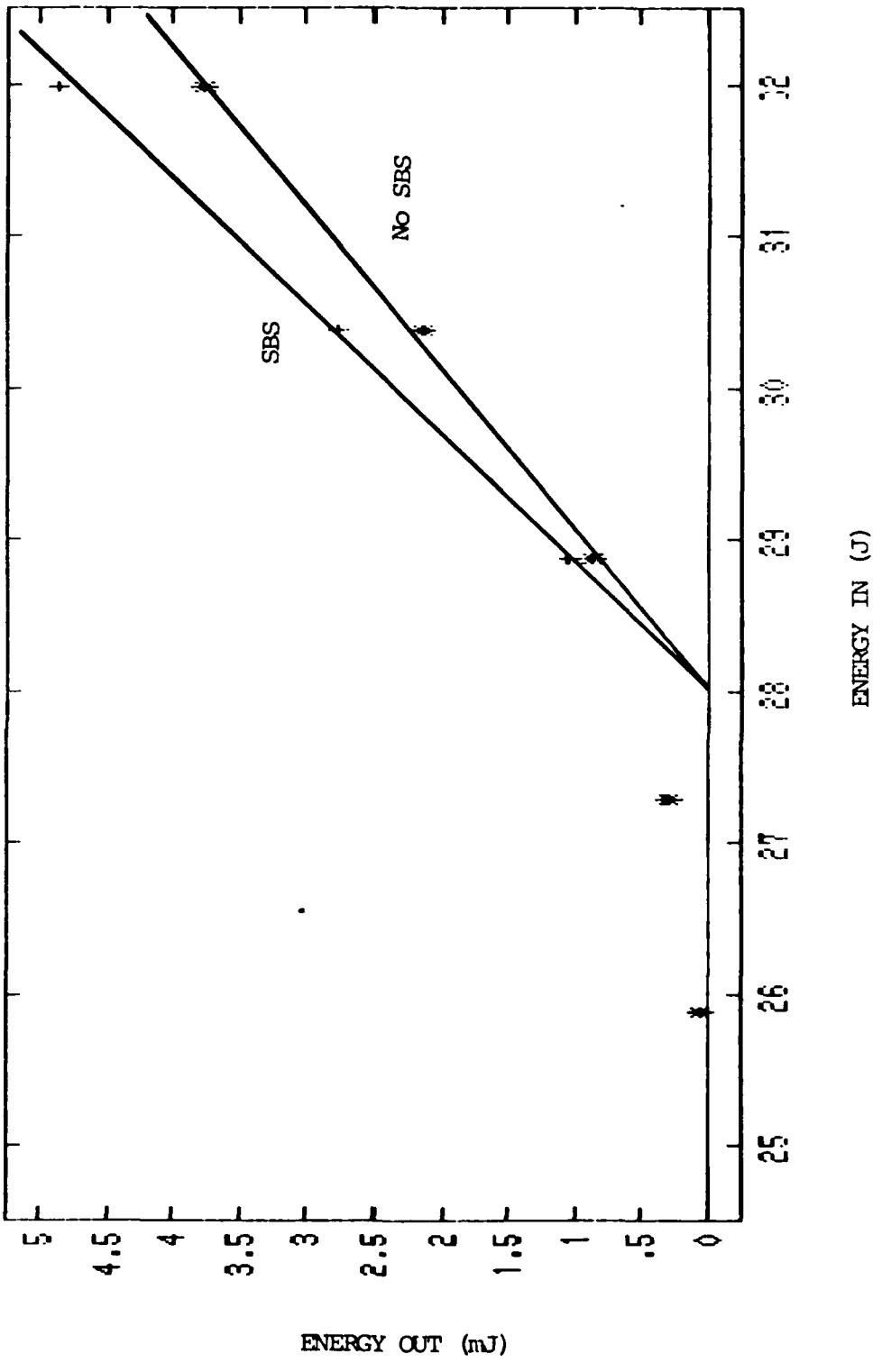

Figure 18 PCR performance with Korad etalon and one element resonant reflector. Ψ-no SBS, Ψ'-with SBS

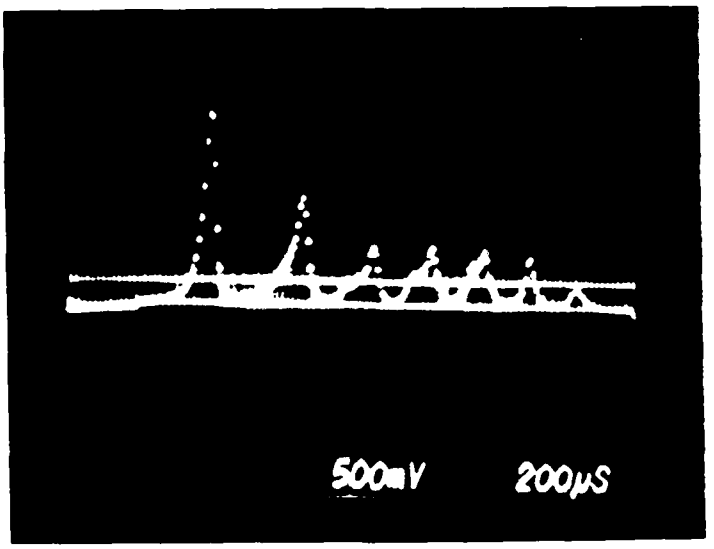

Figure 19 Spectral ouput for Figure 18, no SBS

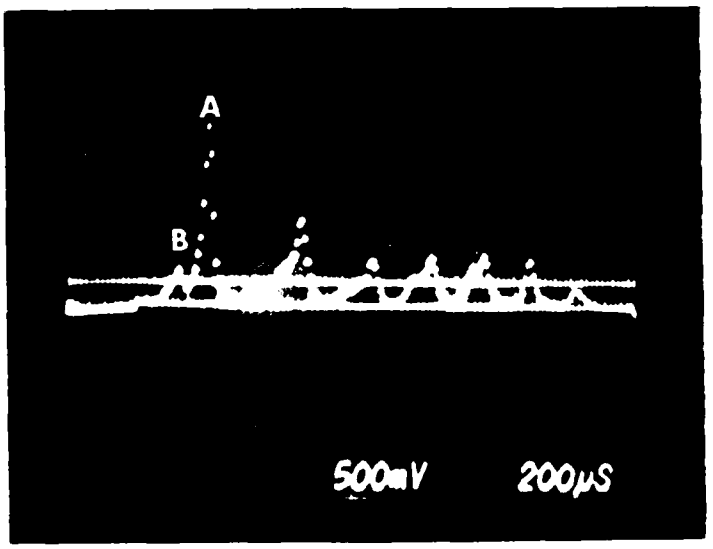

Figure 20 Spectral output for Figure 18, with SBS.
'A'-No SBS, 'B'-SBS shifted.

removed. (With the Korad etalon in the beam quality was particularly poor, and the spectral output very unstable.) The cavity dumped performance is shown in Figure 21. In this case the spectral shift was very pronounced, as shown in Figure 22. The shifted output, labelled 'B' in the figure, dominates because the SBS reflection was higher than the resonant reflector (25% for the resonant reflector and a peak of over 30% for SBS). The shift in all cases was consistent with the theoretical SBS shift.

The spot images for the PCR could be easily observed in this case because of the large SBS reflectivity. The spots were consistently worse with SBS, behaving as though two different cavities were running at the same time, each with its own optimum alignment (see Figures 23 and 24).

Apertured Cavity.

If a cavity is apertured it is expected that the number of transverse modes is reduced, possible to the extent that TEMoo operation may be achieved. In view of the spectral sensitivity of SBS this might be expected to increase the reflectivity achieved from the SBS cell. Although the cavity fluence will be greatly reduced by aperturing, the relative increase of cavity dumped energy between the SBS and non-SBS cases might be better than in the unapertured cavity. In light of this argument measurements were taken on various configurations with apertures, of various sizes, inside the cavity. These apertures were placed as shown in Figure 1.

The first case to be considered was with a high reflector, the Korad etalon, and the one element resonant reflector. The results for 4

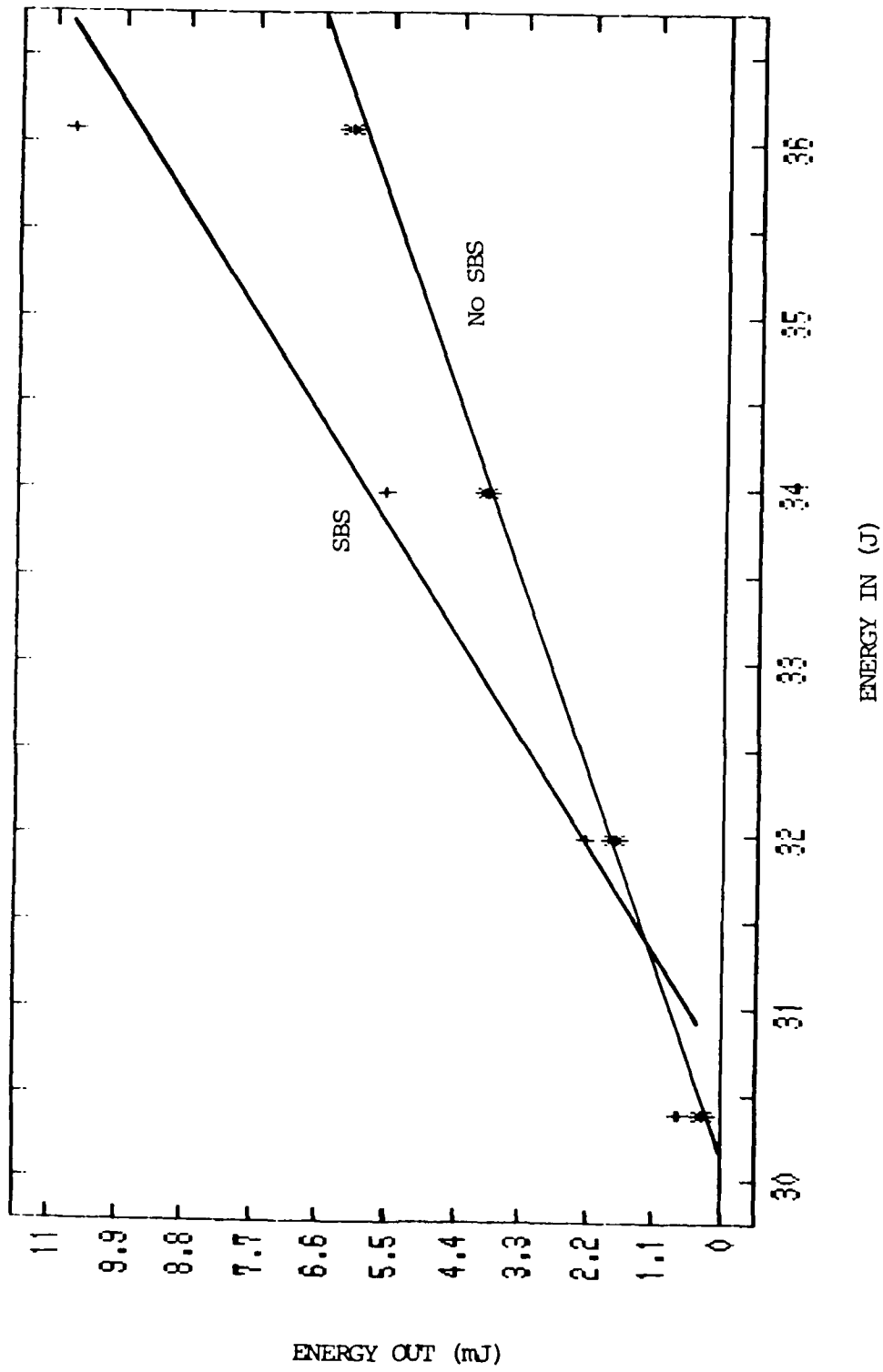

Figure 21 PCR performance with six and one element resonant reflector. ✱-no SBS, ✱-with SBS

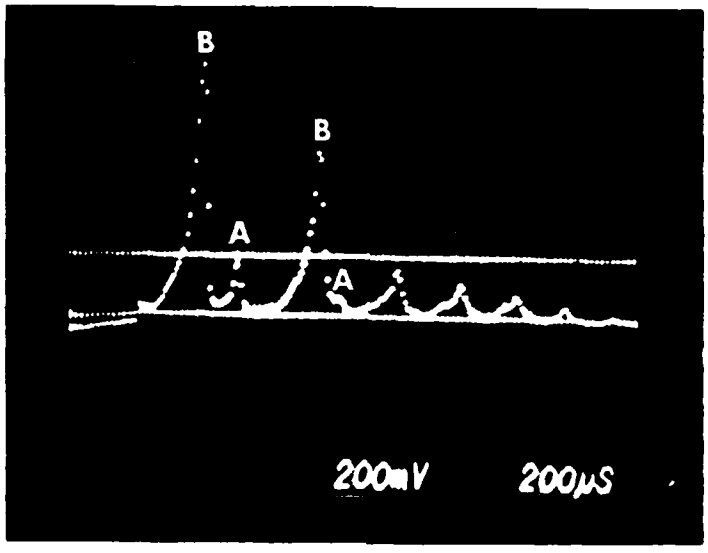

Figure 22 Spectral output for Figure 21, with SBS
'A'-No SBS, 'B'-SBS shifted.

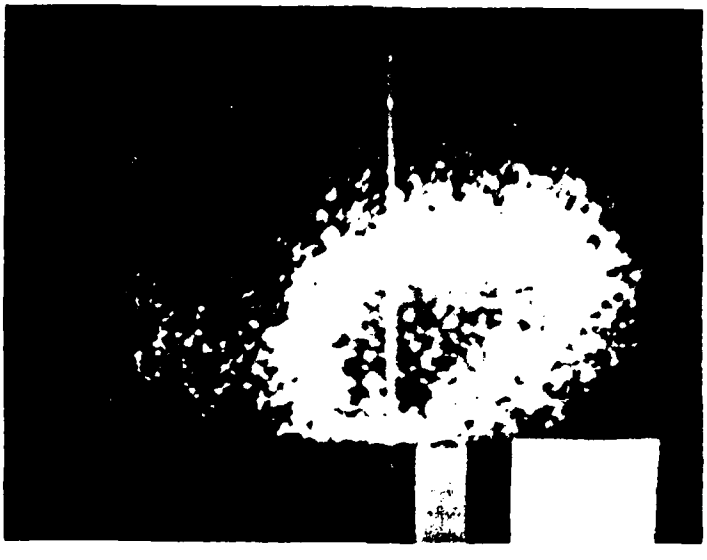

Figure 23 Spot image for Figure 21, no SBS

Figure 24 Spot image for Figure 21, with SBS

milimeter and 2 milimeter diameter apertures are shown in Figures 26 and 27 respectively. Compared to the unapertured cavity, the performance did improve in the case of aperturing, although the output energy was well reduced. The difference in performance increase over the non-SBS case for 2 mm and 4 mm apertures was not appreciable, while the 4 mm case provides much greater output energy for a given energy input to the lamp. The spectral traces, Figures 25 and 28, show the SBS shift, as in previous cases. In the case of aperturing, however, the beam quality remained the same with and without SBS.

With the high reflector replaced with the 6 element resonant reflector, and the Korad etalon removed, the cavity was apertured to 2.5 milimeters diameter. In this case the peak energy output improvement

did not exceed that experienced in the unapertured cavity, and again the beam quality did not change with SBS. In addition there was an unusual roll-off of the energy output, with and without SBS (see Figure 30). The spectral traces also showed unusual properties in that the spectral purity of the SUR was not as good as previously obtained (Figure 29). The double peak in the non-SBS traces, possibly caused by etalon thermal wander, must detrimentally affect the SBS reflectivity but it is not clear how this is related to the roll-off of energy performance in both SBS and non-SBS cases.

Cavity Aberrators.

Two cavity aberrators were employed to investigate the fault tolerance of a PCR. These were an ordinary microscope slide and a wire screen. The effects of these elements could simulate failed optical elements.

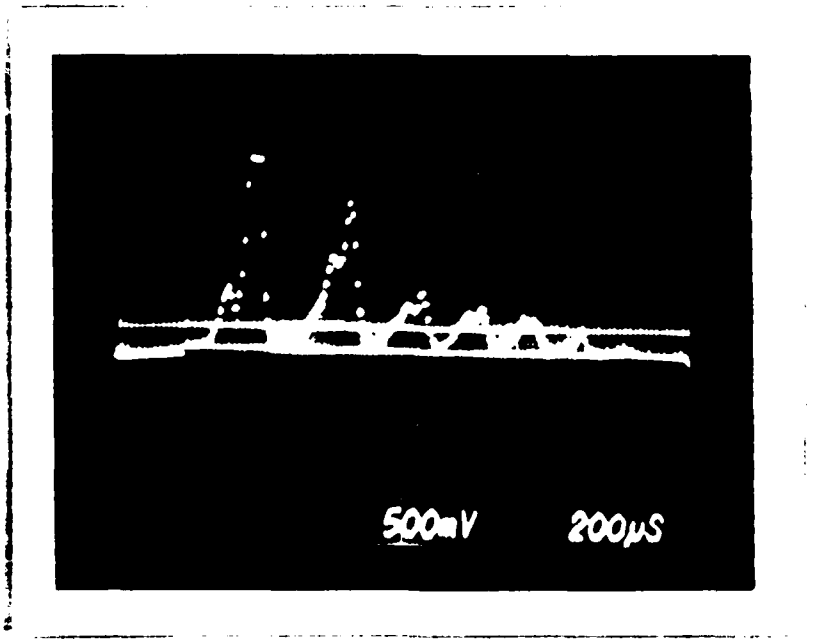

Figure 25 Spectral output for Figure 26, with SBS

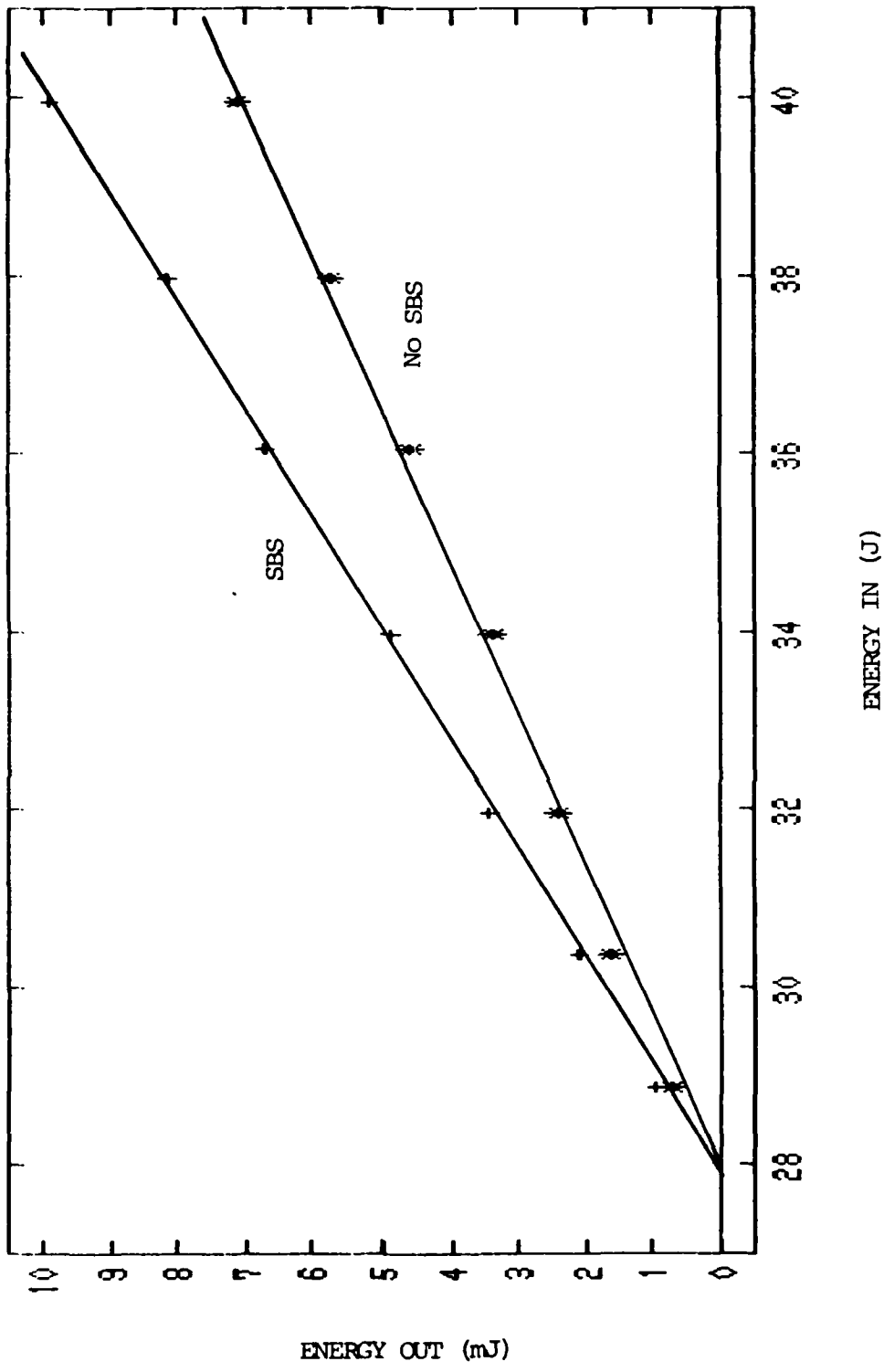

Figure 26 4 m Apertured PCR performance. Normal high reflector, Korad etalon, one element resonant reflector
'*'-no SBS, '+'-with SBS

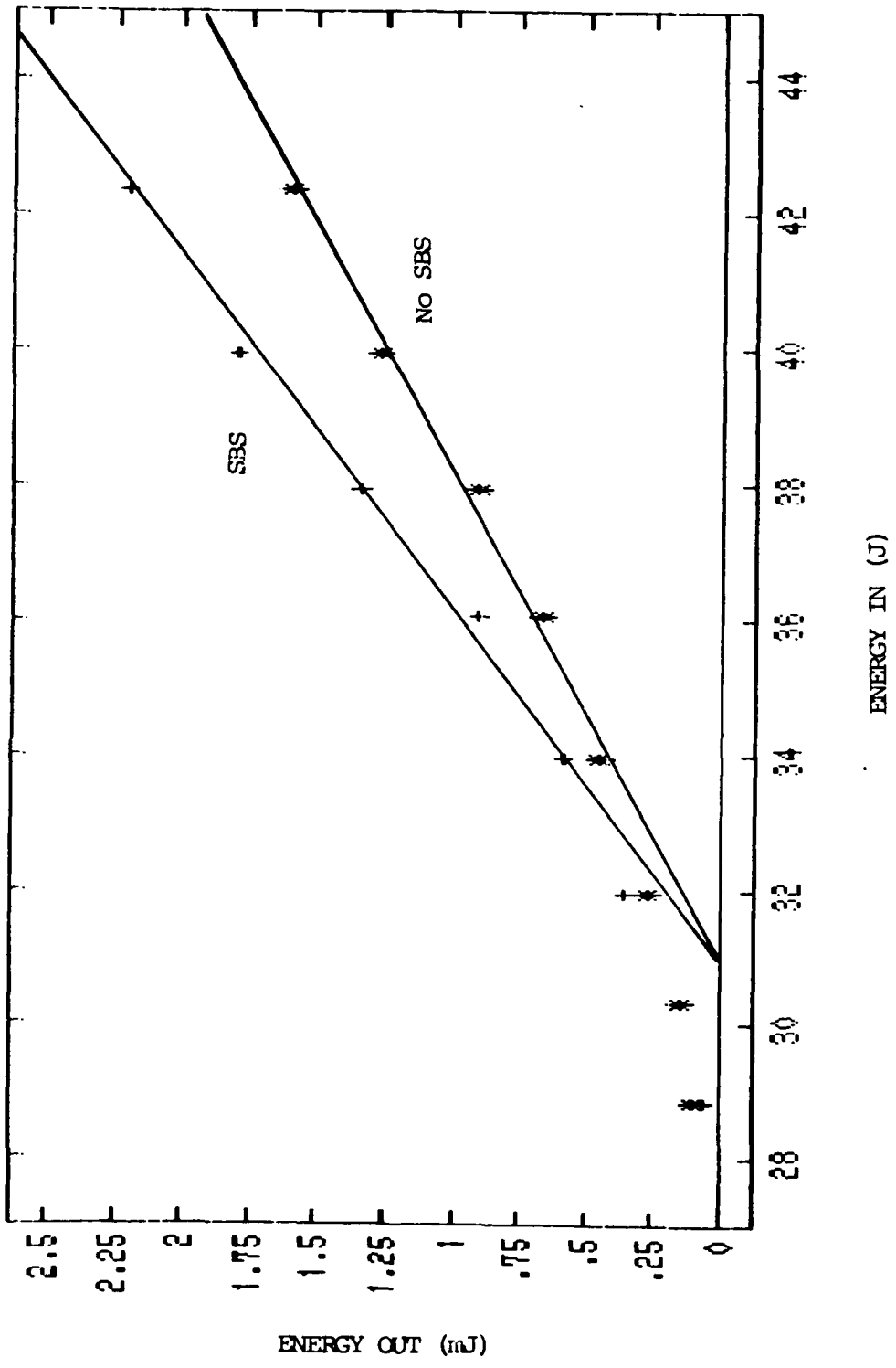

Figure 27 2mm Apertured PCR performance. Normal high reflector, Korad etalon, one element resonant reflector. '*'-no SBS, '+'-with SBS

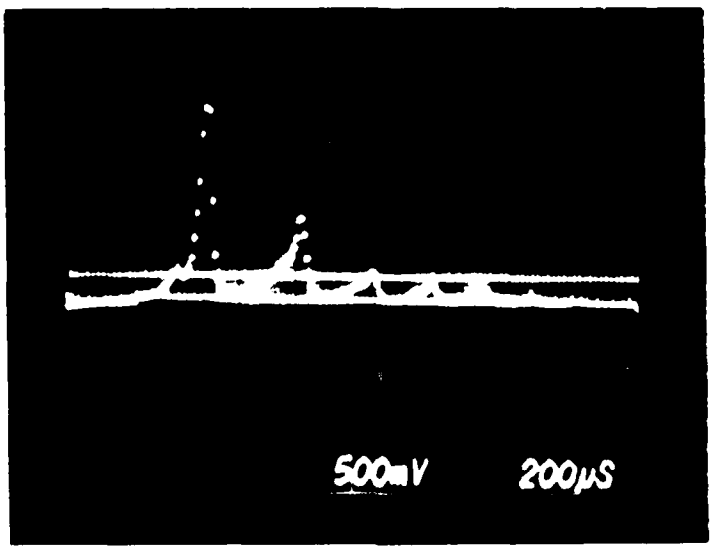

Figure 28 Spectral output for Figure 27, with SBS

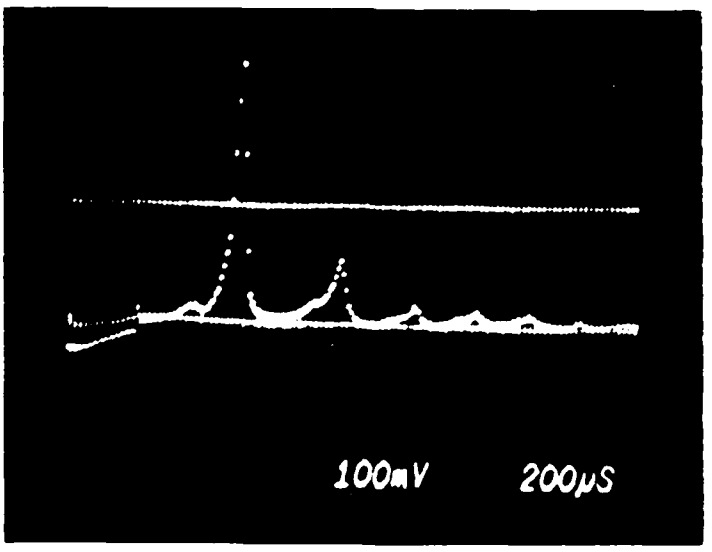

Figure 29 Spectral output for Figure 30, no SBS

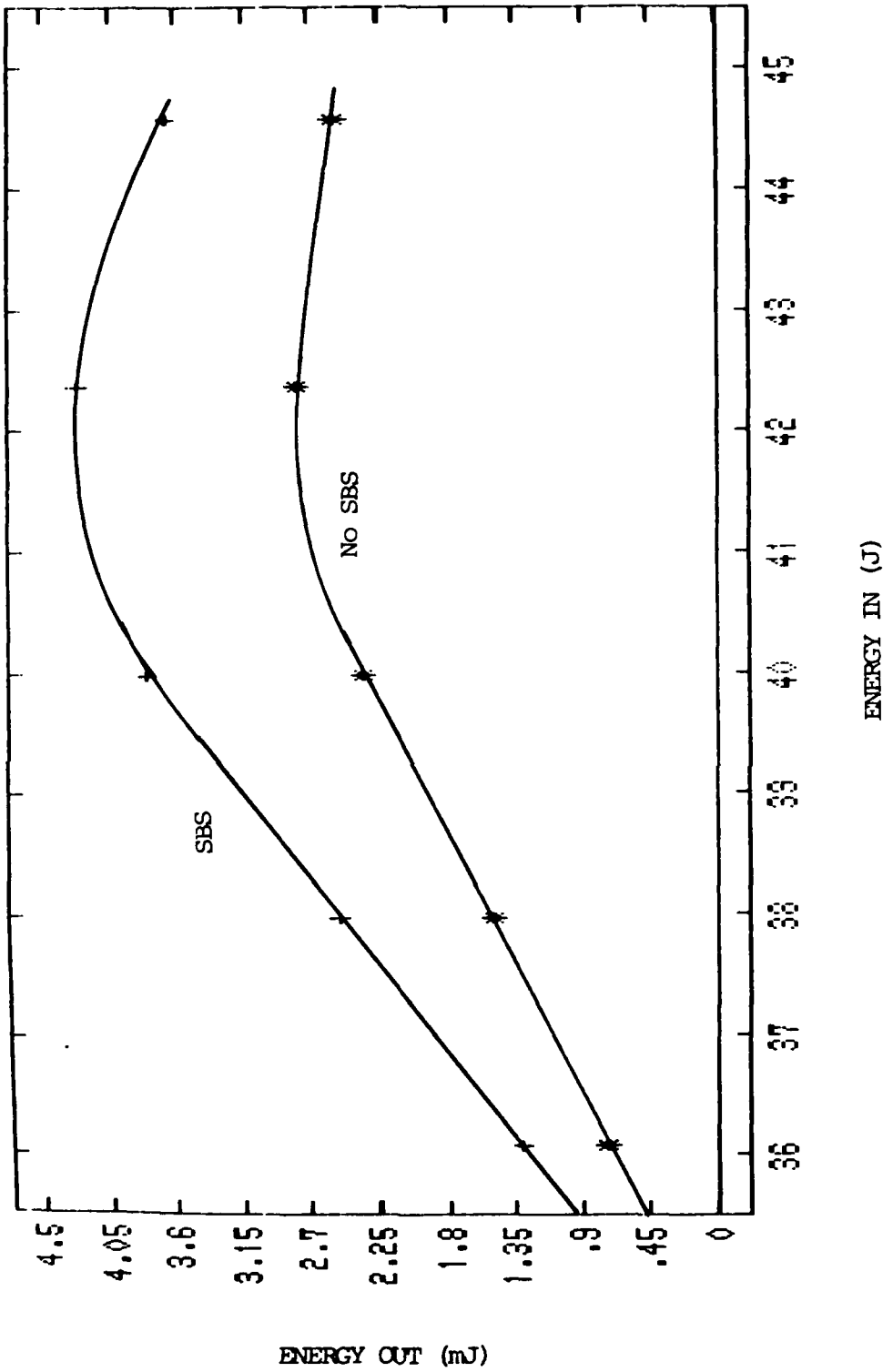

Figure 30 2.5mm Apertured PCR performance. Six and one element resonant reflectors. Ψ-no SBS, Ψ-with SBS

The wire screen was placed between the Q-switch and the output coupler, as this was the only position in the cavity where space was available. The effect on SUR performance was dramatic, especially the spot image. The results for normal high reflector, Korad etalon, and one element resonant reflector are shown in Figure 31. The results for the six element resonant reflector high reflector and one element resonant reflector output coupler are shown in Figure 32. The spot images associated with Figure 32 are shown in Figures 33 and 34. There was little change in beam quality, although output energy performance was improved substantially.

The cavity dumped energy performance experienced a roll-off, similar to that experienced for the aperture case discussed above. The spectral purity of the two-resonant-reflector SUR cavity, Figure 35, might be related to this, but the spectral impurity was not obvious for the normal high reflector-Korad etalon-resonant reflector cavity.

The microscope slide was placed in the same position as was the wire screen. The results for the two cavities discussed for the wire screen are shown in Figures 37 (high reflector-Korad etalon-resonant reflector) and 38 (two resonant reflectors). The improvement in cavity dump energy was, again, quite pronounced, but the most interesting feature was the spectral output of the two cavities. The cavity with a normal high reflector exhibited many peaks, all seperated by the SBS frequency shift (Figure 36). The resonant-reflector-high-reflector cavity exhibited mutiple shifted peaks also, but there were fewer peaks and they appeared to be suppressed (Figure 39). The reasons behind this behavior will be discussed later in Section V.

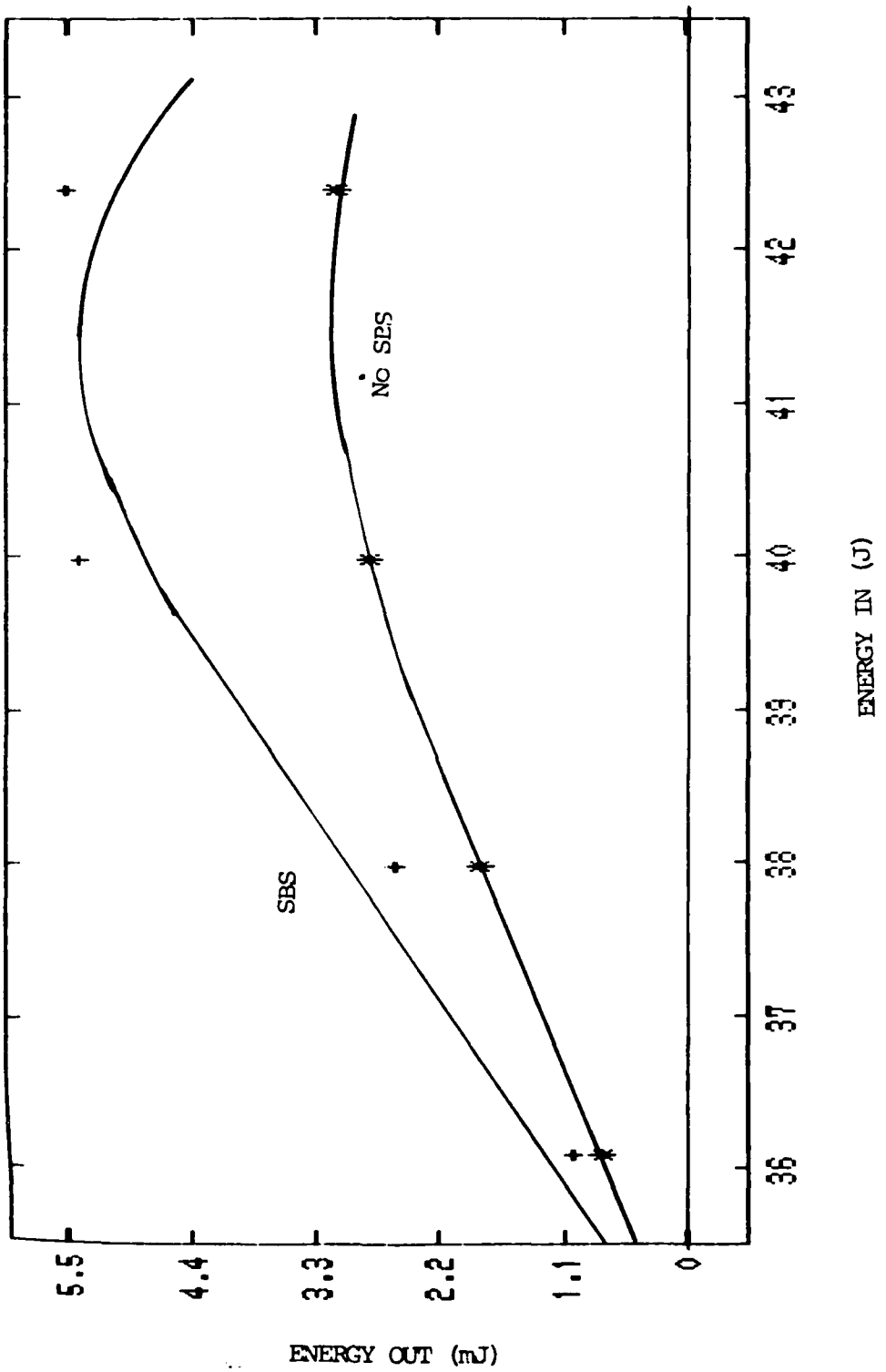

Figure 31 PCR performance with wire screen aberrator. Normal high reflector, Korad etalon, one element resonant reflector. ✱'-no SBS, 4'-with SBS

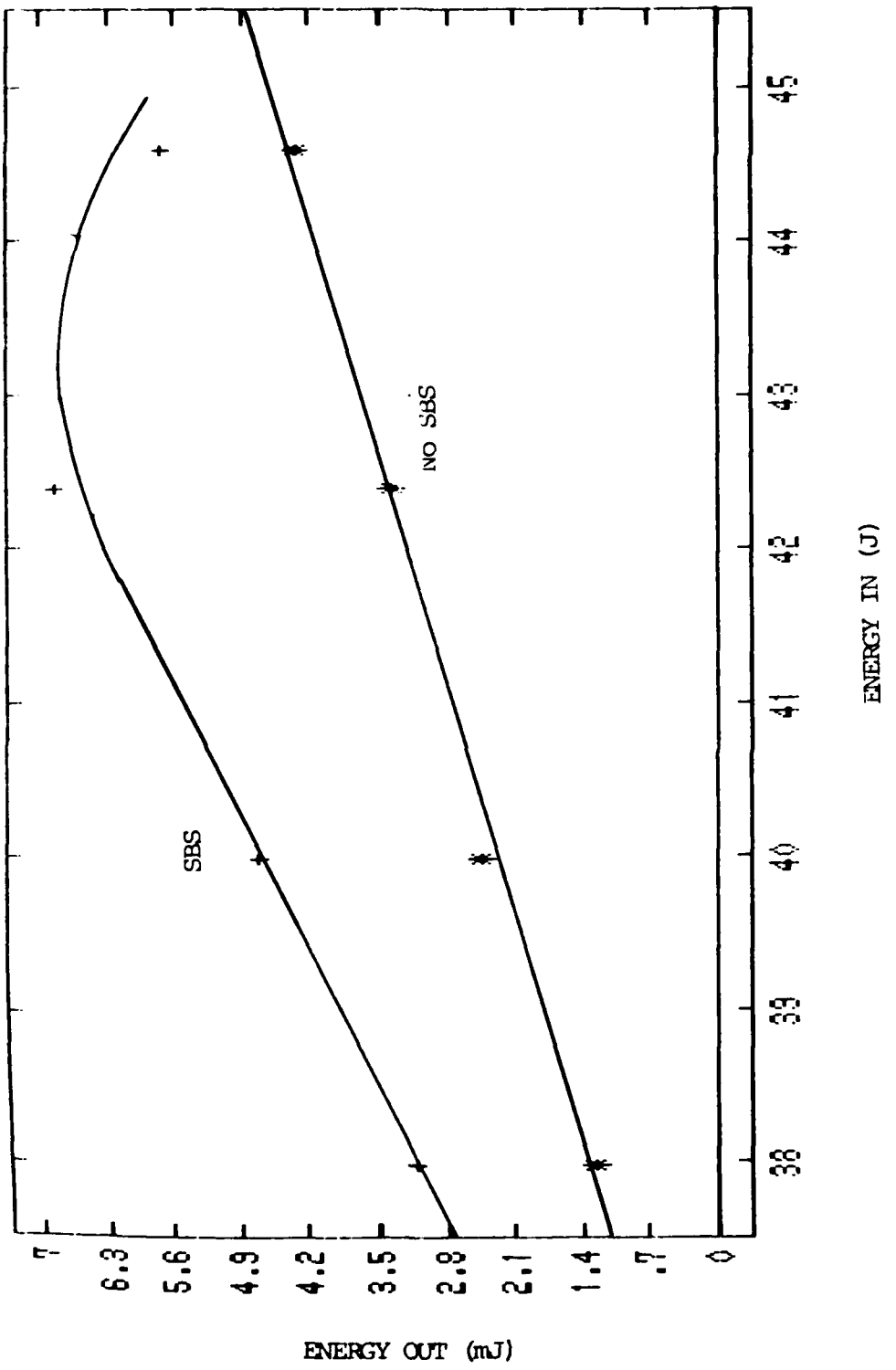

Figure 32 PCR performance with wire screen aberrator. Six and one element resonant reflectors. '*'-no SBS, '+'-with SBS

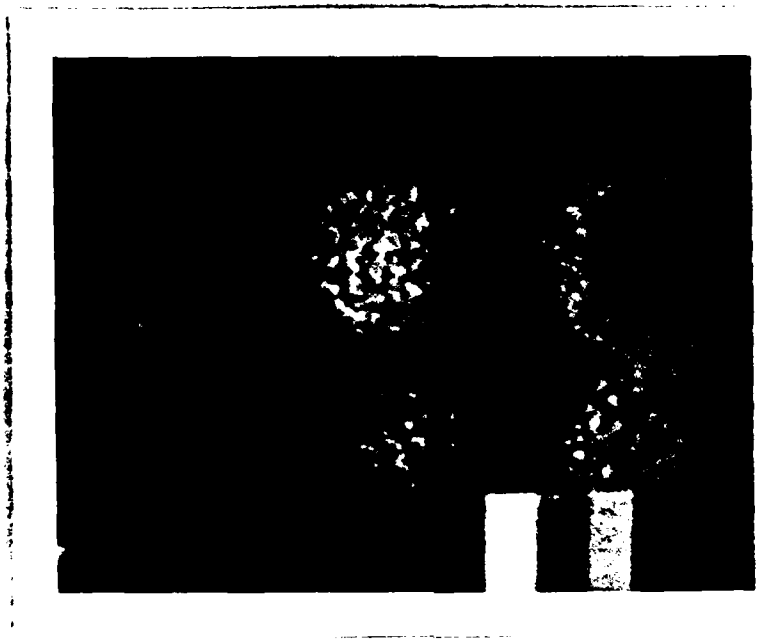

Figure 33 Spot images for Figure 32, no SBS

Figure 34 Spot image for Figure 32, with SBS

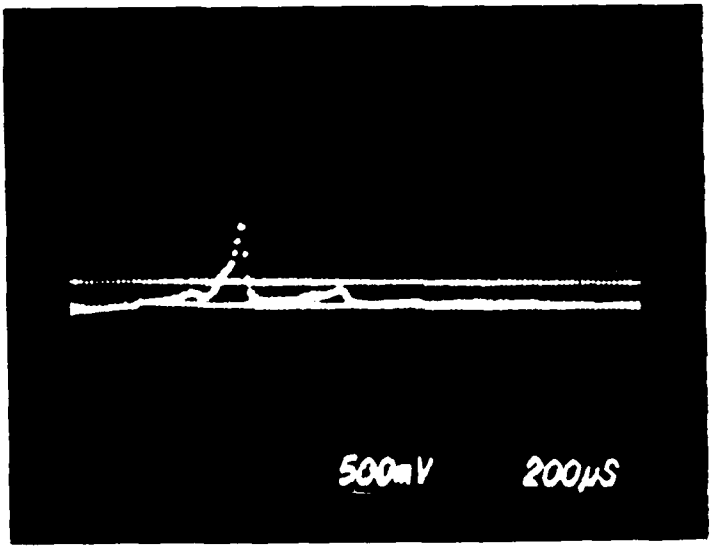

Figure 35 Spectral output for Figure 32, no SBS

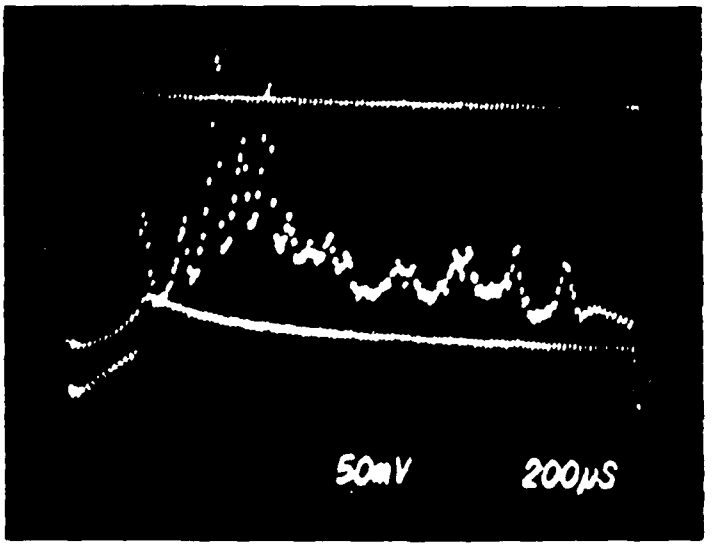

Figure 36 Spectral output for Figure 37, with SBS

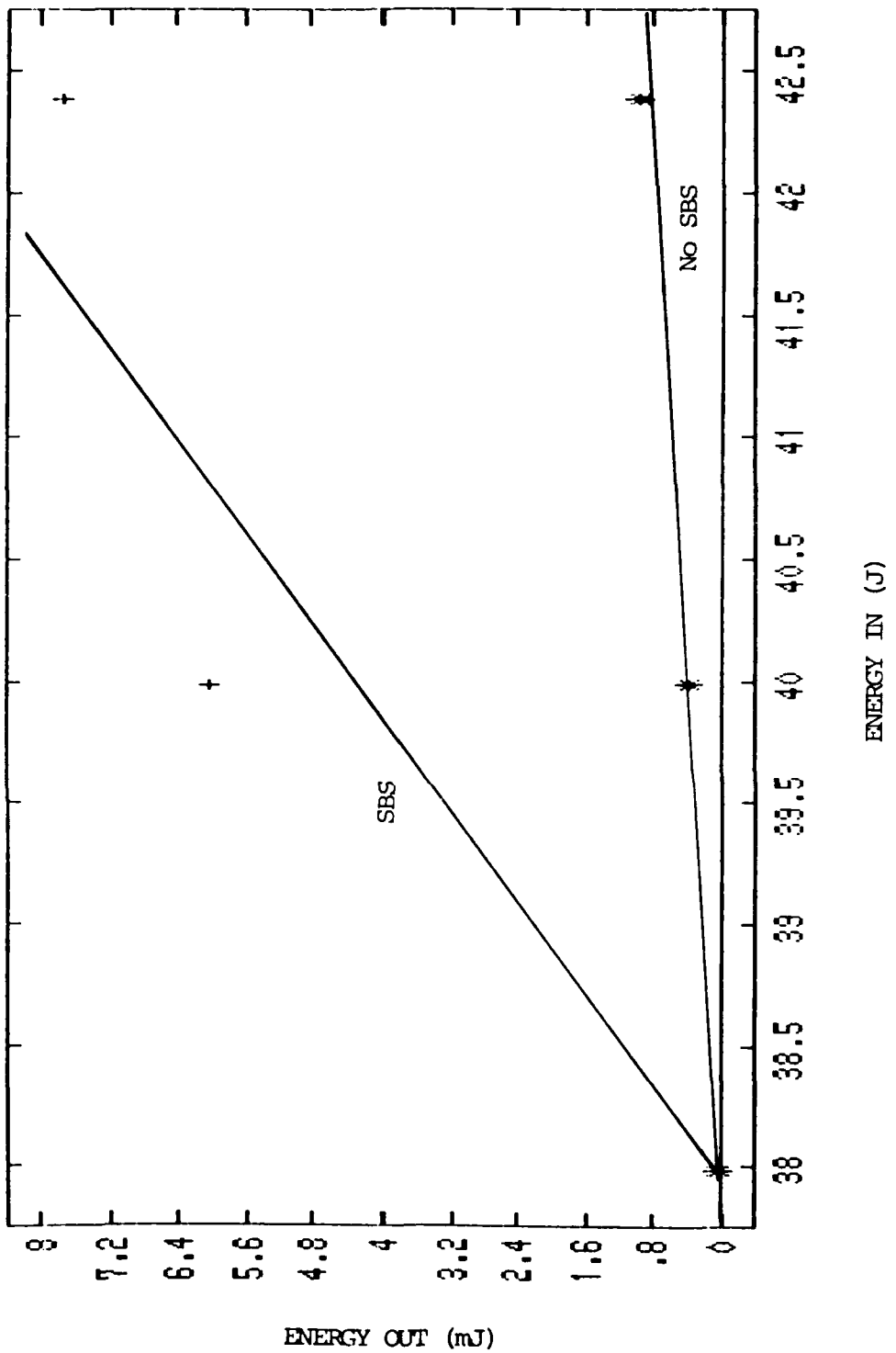

Figure 37 PCR performance for microscope slide aberrator. Normal high reflector, Korad etalon, one element resonant reflector. '*'-no SBS, '+'-with SBS

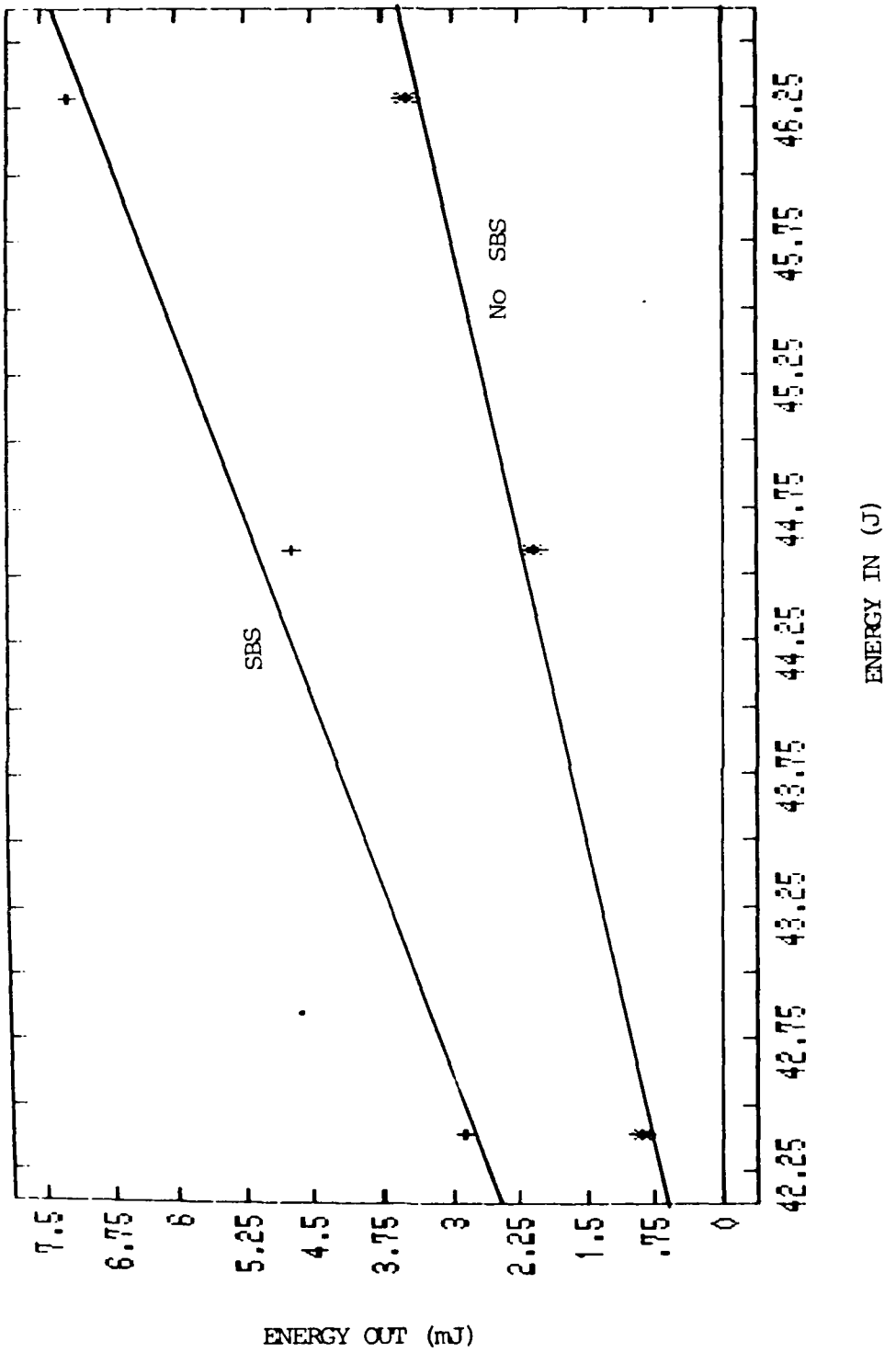

Figure 38 PCR performance for microscope slide aberrator. Six and one element resonant reflectors.
'*'-no SBS, '+'-with SBS

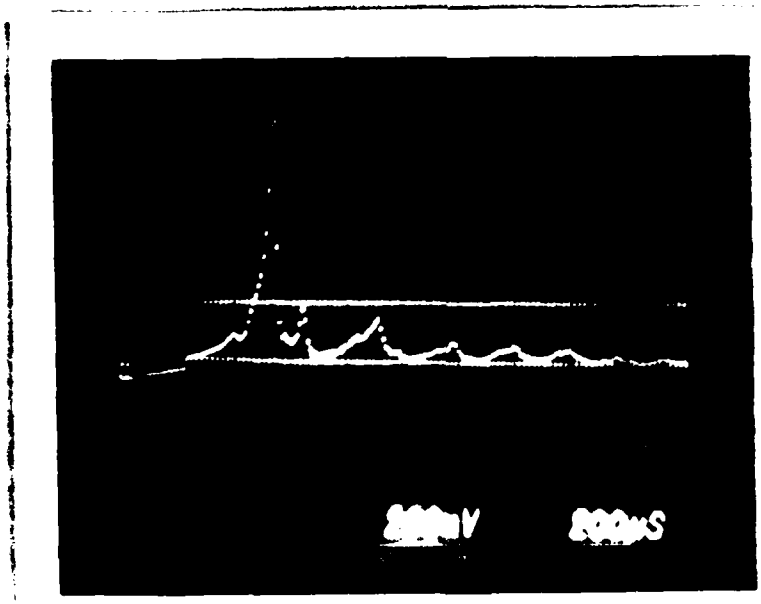

Figure 39 Spectral output for Figure 38, with SBS

Notably, the results for a misaligned cavity were quite similar.

It was again apparent that the beam profile suffered with the addition of SBS. Figures 40 and 41 show the two different spots. This is consistent with the results for the wire screen, and for the unaberrated cavity.

Misaligned Cavity

The misalignment of the cavity was obtained by angular adjustment of the output coupler by 4 miliradians in the horizontal axis. This resulted in filamentary operation of the SUR, and an increased threshold.

The results for normal high reflector are shown in Figure 42, while the results for six element resonant reflector high reflector are shown

in Figure 43. Each graph includes a trace of the aligned cavity performance for reference. The PCR improved performance for cavity dumped energy out, but again the spectral output was unusual.

The results were very similar to that for the case of the microscope slide inserted in the cavity. The normal high reflector case showed many SBS shifted peaks (Figure 44). The cavity with the resonant reflector as high reflector had only one shifted peak (Figure 45).

The spot images were again worse with the SBS (Figures 46 and 47). The structure in the spots is due to interference associated with the resonant reflector output coupler misalignment.

Figure 40 Spot images for Figure 38, no SBS

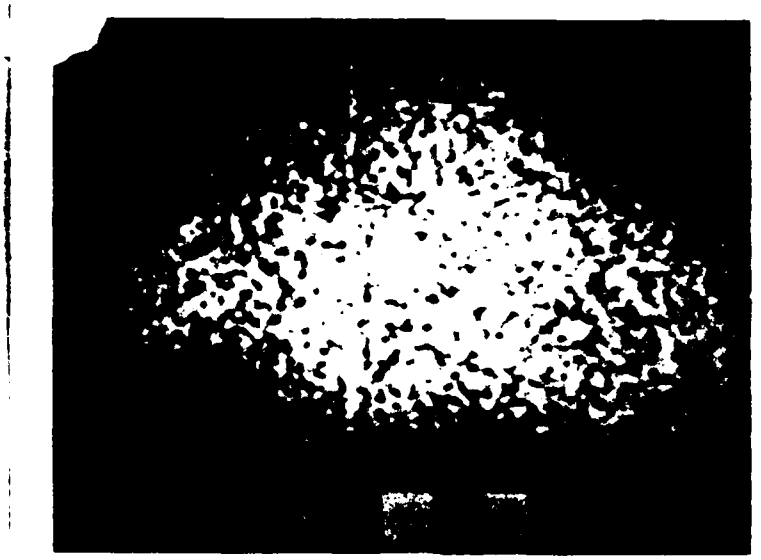

Figure 41 Spot image for Figure 38, with SBS

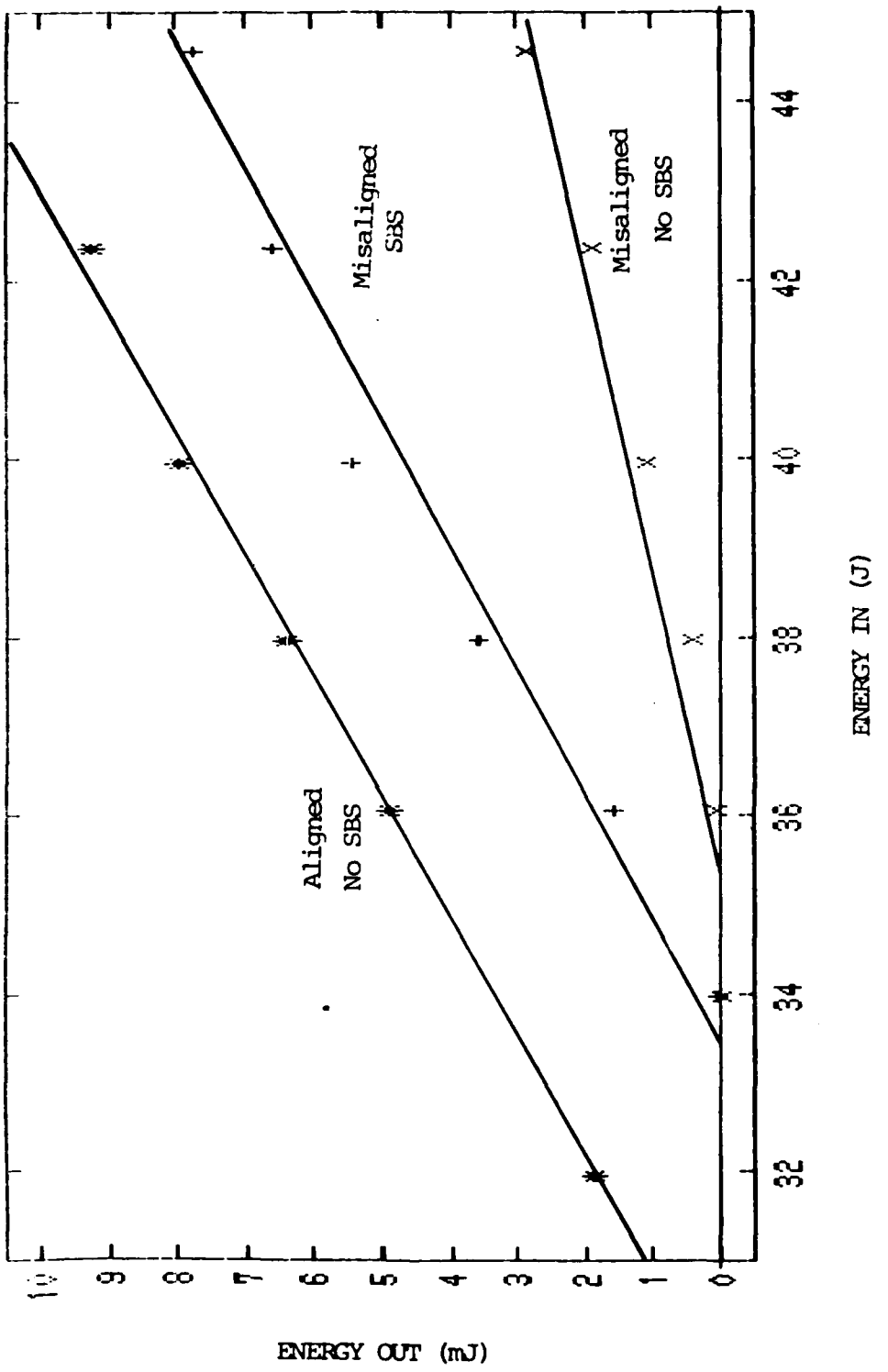

Figure 42 PCR performance for misaligned SUR. Normal high reflector, Korad etalon, one element resonant reflector. '*'-no SBS, '+'-with SBS

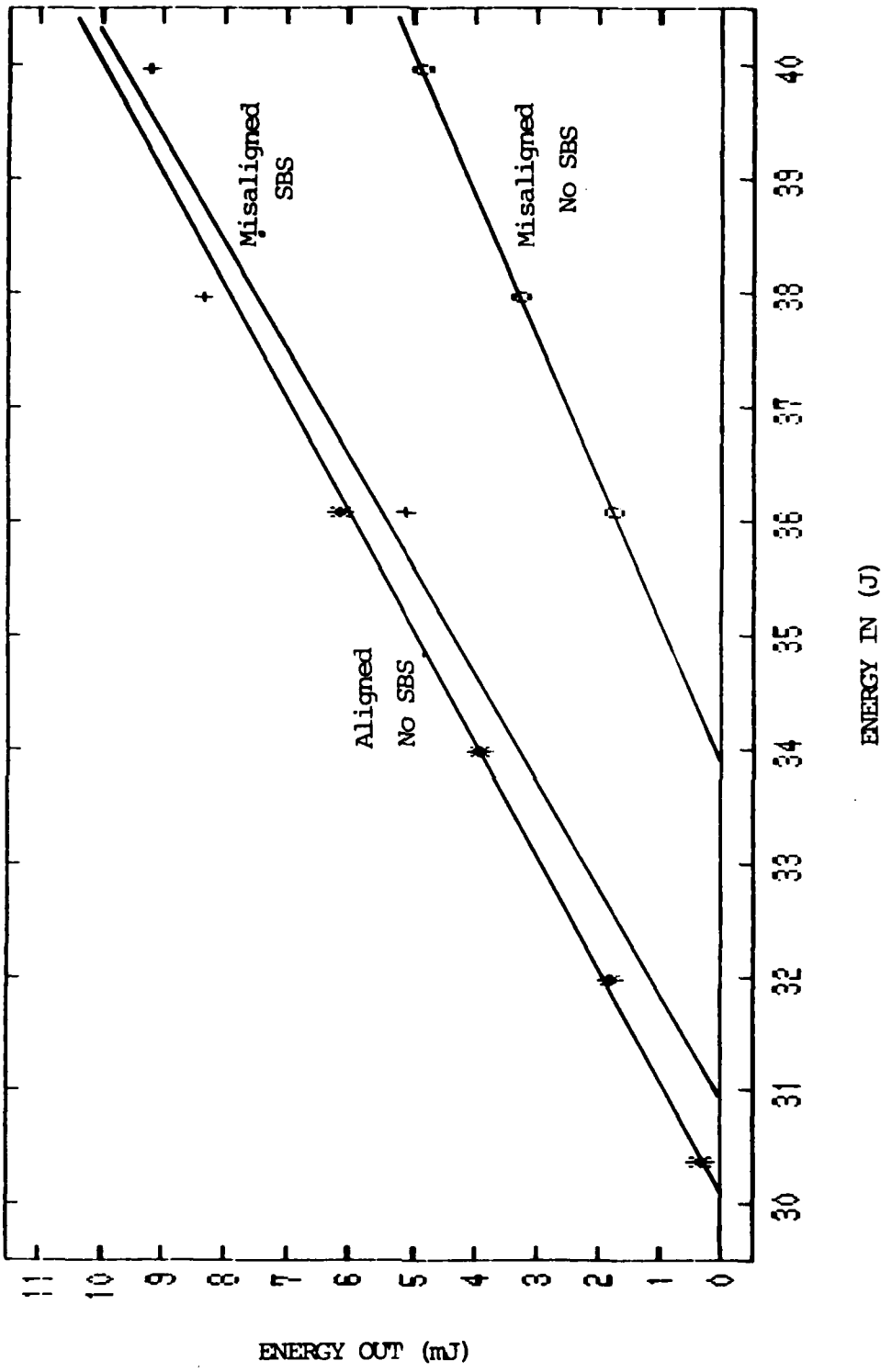

Figure 43 PCR performance for misaligned SUR. Six and one element resonant reflectors.
'O'-no SBS, 'Ψ'-with SBS

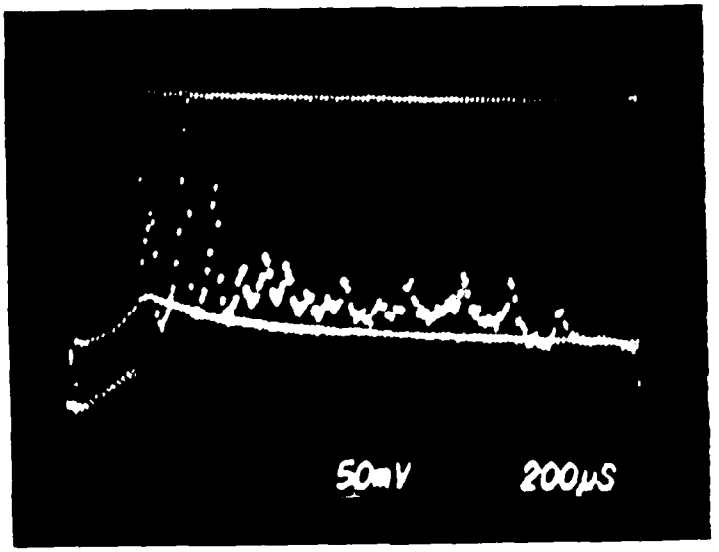

Figure 44 Spectral output for Figure 42, with SBS

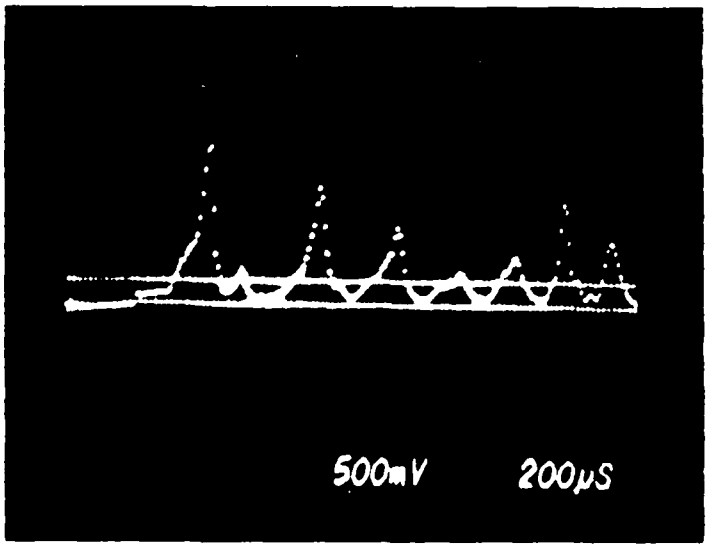

Figure 45 Spectral output for Figure 43, with SBS

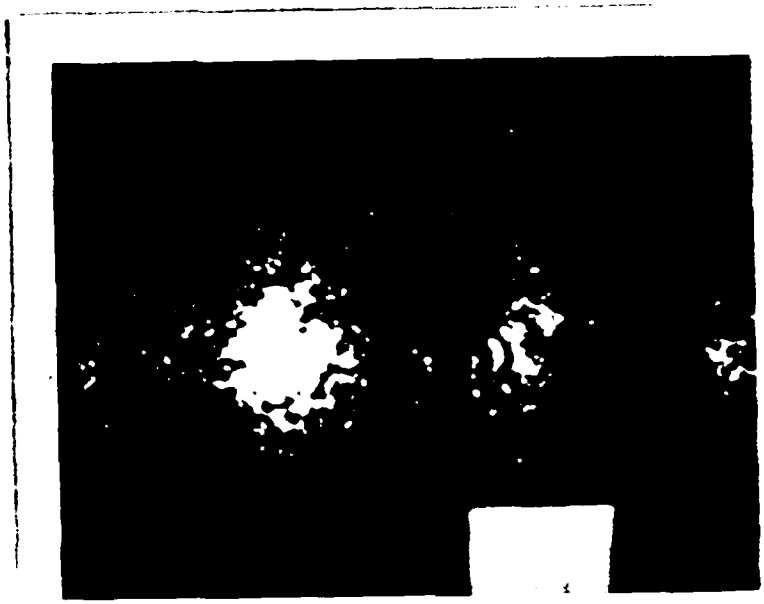

Figure 46 Spot image for Figure 43, no SBS

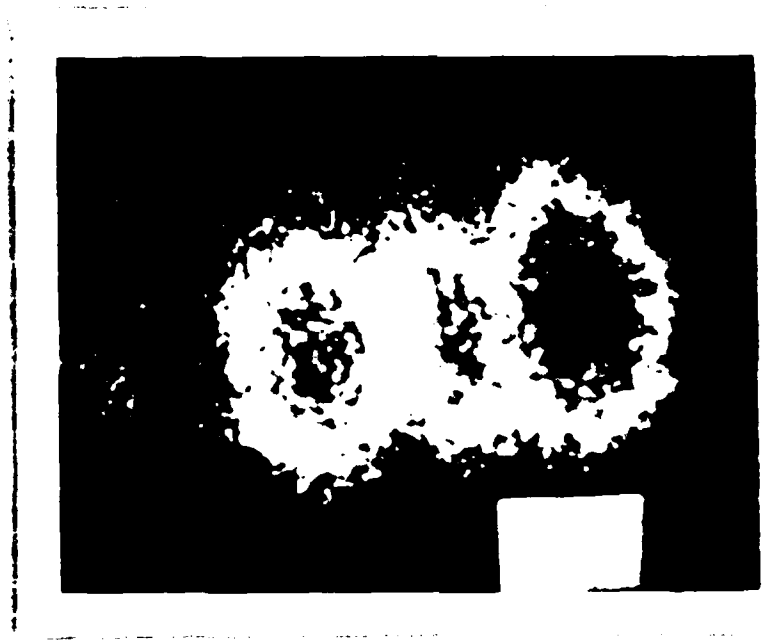

Figure 47 Spot image for Figure 43, with SBS

V. Discussion of Results, Conclusions, and Recommendations.

Discussion of Results.

The overall results are summarized in Table I.

Energy Output.

In cases where SBS was achieved the output energy performance of the PCR increased. This is due to a simple net increase in the reflectance of the output coupler end of the cavity. In some cases it was also due to an increase in the mode volume utilization, as with cavity misalignment. If the reflectivity of the SBS could approach 100% then the performance of the PCR could exceed that of a cavity dumped resonator with 100% conventional mirrors, due to the increased mode volume utilization. This was not nearly the case in the work reported in this thesis.

The overall energy output performance was hindered by factors associated with both the SUR and the SBS medium. For practical reasons the SUR was never able to operate TEMoo. If the SUR was apertured to the extent that TEMoo was achieved, there was not enough fluence to initiate the SBS. Multi-transverse mode operation is not conducive to high SBS reflectivity, but in this experimental case it was the only means to achieve the fluence necessary to produce any SBS.

SBS reflectivity is also greatly enhanced by limiting the number of longitudinal modes of the SUR. Ideally, single longitudinal mode (SLM) operation is desired. Although the spectral linewidth of the SUR was reduced by the use of etalon elements, SLM was not nearly achieved. The control and equipment necessary to produce SLM, or nearly SLM, operation was not available.

TABLE I
SUMMARY OF EXPERIMENTAL RESULTS

CASE	ETALON ELEMENTS	THRESHOLD (J)		SLOPE EFF. (mJ/J)		SPOT QUAL.
		SBS	No SBS	SBS	No SBS	w.r.t. No SBS
SUR only						
100% OC			20.1		2.38	
45% OC			23.9		1.97	
35% OC			24.4		1.78	
27% OC			27.5		2.07	
Three mirror SUR only						
45, 35, 27% OC			21.9		2.27	
Aligned						
	Korad	26.3	26.3	1.62	1.49	worse
	Korad, 2 element	26.4	26.2	1.46	1.23	worse
	Korad, 1 Res. Ref.	28.0	28.0	1.22	.94	worse
	2 Res. Ref.'s	31.0	30.3	2.06	1.07	worse
Apertured						
4mm AP	Korad, 1 Res. Ref.	27.8	28.2	.806	.591	same
2mm AP	Korad, 1 Res. Ref.	31.3	31.2	.200	.141	same
2.5mm AP	2 Res. Ref.'s	34.1	34.4	.644	.418	same
Aberrated						
Slide	Korad, 1 Res. Ref.	37.5	38.0	1.72	.205	worse
Slide	2 Res. Ref.'s	39.9	41.2	1.10	.658	worse
Wire Screen	Korad, 1 Res. Ref.	35.4	34.6	1.13	.531	worse
Wire Screen	2 Res. Ref.'s	34.3	35.0	.851	.460	worse
Misaligned	Korad, 1 Res. Ref.	33.6	35.2	.745	.273	worse
Misaligned	2 Res. Ref.'s	30.9	33.8	1.05	.794	worse

Key: (See section II) "Korad" - Korad etalon, "2 element" - 2 element etalon, "1 Res. Ref." - 1 element resonant reflector used as output coupler, "2 Res. Ref." - 1 element resonant reflector used as output coupler and 6 element resonant reflector used as high reflector.

Given these factors, the best SBS reflectivity achieved was 40%, obtained using two resonant relectors and an unapertured cavity. In the case of an aberrated cavity the best compensation achieved was energy output just over that of the unaberrated and non-SBS SUR (for the misaligned cavity whose performance is shown in Figure 43).

The spectral shift produced upon SBS reflection from carbon disulfide also detrimentally affected the energy output performance. The large shift permitted only one SBS reflection to experience gain under most operating conditions; higher order reflections were shifted out from under the gain linewidth.

SBS Shift.

The Fabry-Perot traces observed when SBS was active showed the spectrally shifted output of the PCR. The shift calculated using the traces, .12 cm^{-1} , corresponds well with the theoretical value of .126cm^{-1}. In the case of an aligned and unaberrated cavity only one shifted peak was seen. This is due to the fact that the startup resonator operates before the PCR, and hence the gain medium has already been depleted to some extent. This causes a relatively narrow gain linewidth from which shifted peaks may extract. This is aggravated by the large value of the SBS shift for carbon disulfide. Hence, only one shifted peak may be supported by the cavity.

When the gain is not extracted very well by the SUR, such as when the cavity is misaligned or when a microscope slide is placed in the cavity, the SUR has a very high threshold. A larger inversion and a broader gain linewidth is available when the SBS begins and the threshold suddenly drops. Now several shifted lines may be supported.

This effect was pronounced for the conventional high reflector, but less so for the six element resonant reflector used as the high reflector. This is due to the wavelength selectivity of the resonant reflector. Although the first shifted line is reflected by about 30% (see Figure 6), the second line is less than 10% reflected. This, coupled with being in the wings of the gain linewidth, prevents more than a single shifted line being present in the resonant reflector case.

Spectral Purity.

The introduction of etalon elements into the SUR, including resonant reflectors, had a pronounced effect on the reflectivity of the SBS cell. Qualitatively, the line narrowing effects of the elements could be seen on the Fabry-Perot, and the narrowing corresponded to an increase in PCR performance. It was found that when the SUR drifted from narrow line output in a given experimental setup, as in the case of two spectral peaks, the PCR performance suffered.

Spot Quality

At the very best the spot quality of the PCR was about the same as the SUR. This was the case with an apertured cavity. In general though, the transverse mode properties of the PCR were much worse than that of the SUR without the SBS. This seems to be predicted in theory for the case of large SBS shift. In order to have a higher quality PCR beam measures must be taken to carefully control the transverse mode properties of the SUR, the least of which should be TEMoo operation. The measures that would ensure low order stable transverse mode operation of the PCR are unclear, especially with cavity aberrations that produce multi-transverse SUR operation, but the use of an SBS medium with a very

much smaller frequency shift should simplify the PCR in this respect.

Conclusions.

The construction of a three mirror collinear PCR met with mixed results. The PCR worked well in increasing output given a particular output coupler, and worked very well in increasing fault tolerance. The addition of aberrators, particularly the microscope slide, and the misalignment of the cavity was well compensated for by the SBS reflection. This could be an important result for laser applications where laser output reliability is paramount, without particular respect to beam degradation and spectral purity, and the need to reduce manufacturing tolerances in the production of laser sources.

The particular setup used, including the carbon disulfide and poor SUR beam quality, produced a PCR with poor transverse mode properties and spectral purity. This should be improved with higher quality SURs, an SBS medium with a very small shift, and the corresponding transverse and longitudinal mode control of the SUR. The requirement to have such a highly controlled SUR may prevent the PCR from ever being fault tolerant. An aberrated SUR could prevent the PCR from desirable operation. The very nature of SBS may cause problems with respect to spectral purity even if the SBS shift is small. Processes that require narrow linewidth, such as nonlinear interactions, may preclude the use of any SBS based PCR.

Recommendations.

The investigations into an SBS PCR should be continued with improved equipment that can ensure a high degree of control on the properties of the SUR. In addition, the PCR should make use of an SBS

medium with a very small frequency shift. If the penalty in energy efficiency can be afforded, a degenerate four wave mixing PCR should be considered. There may be other PCR configurations which might promote better operating characteristics, and thus attain the fault tolerance and increased performance that are the selling points of a phase conjugate mirror in a resonator. Any following investigation should be pointed at determining if a PCR is indeed a practical or desirable device to pursue.

Bibliography

1. Auyeung, J. et al. "A theoretical and Experimental Investigation of the Modes of Optical Resonators with Phase-Cojugate Mirrors," IEEE J. Quant. Elec. QE-15(10) (Oct. 1979)

2. Basov, N. et al. "Powerful Laser System with Phase Conjugation by SMBS Mirror," Appl. Phys. 20 (1979)

3. Bel'dyugin, I.M. et al. "Theory of Resonators with Wavefront-Reversing Mirrors," Sov. J. Quant. Elec. 9 (9) (Sept. 1979)

4. Chu, B. Laser Light Scattering, New York: Academic Press, 1974

5. Drummond, P.D. et al. "Specular Reflection in an Interferometer with a Phase-Conjugate Mirror," J. Appl. Phys. 54 (10) (Oct. 1983)

6. Fu, T. et al. "Effects of Signal Detuning on Phase Conjugation," Opt. Let. 4 (11) (Nov. 1979)

7. Giuliani, G. et al. "Transverse Modes of a Stimulated Scattering Phase-Conjugate Resonator," Appl. Opt. 21 (20) (Oct. 1982)

8. Grynberg, G. et al. "Phase Conjugation with Gaussian Beams," Opt. Comm. 47 (4) (sep. 1983)

9. Koechner, W. Solid-State Laser Engineering, New York: Springer Verlag, 1976

10. Lax, M. et al. "Transverse-Mode Descrimination in Three Mirror Resonators," J. Opt. Soc. Am. 63 (12) (Dec 1973)

11. Lehmberg, R.H. "Numerical Study of Phase Conjugation in Stimulated Brillouin Scattering from an Optical Waveguide," J. Opt. Soc. Am. 73 (5) (May 1983)

12. Lind, R.C. et al "Demonstration of the Longitudinal Modes and Aberration-Correction Properties of a Continuous-Wave Dye Laser with a Phase-Conjugate Mirror," Opt. Let. 6 (11) (Nov 1981)

13. Lugovoi, V.N. et al. "Stimulated Mandel'shtam-Brillouin Emission ia an Optical Resonator," Sov. Phys. JETP 15 (4) (Oct 1972)

14. McFarlane, R.A. et al. "Phase Conjugate Optical Resonator," Final Report AFOSR Contract F49620-80-C-0041, Nov. 1983

15. Morse, P.M., Ingard, K.U. Theoretical Acoustics New York: McGraw Hill 1968

16. Muys, P. et al. "Pitfalls in the Use of Equivalent Resonators," Appl. Opt. 21 (22) (Nov. 1982)

17. Pepper, D.M. "Nonlinear Optical Phase Conjugation," Opt. Eng. 21 (2) (Mar.-Apr. 1982)

18. Sato, T. et al. "Stabilization of the BSO Phase Conjugation Using a Feedback Technique," Appl. Opt. 22 (13) (Jul. 1983)

19. Siegman, A.E. An Introduction to Lasers and Masers New York: McGraw-Hill, 1971

20. Starunov, V.S. et al. "Stimulated Mandel'shtam-Brillouin Scattering and Stimulated Entropy (Temperature) Scattering of Light," Sov. Phys. USP 12 (4) (Jan.-Feb. 1970)

21. Yariv, A. Quantum Electronics 2nd Edition, New York: John Wiley and Sons, 1975

22. Yeh, P. "Theory of Phase Conjugate Oscillators," J. Opt. Soc. Am. 2 (5) (May 1985)

23. Zel'dovich, B.Ya. et al. "Phase Conjugation in Stimulated Scattering," Sov. Phys. USP 25 (10) (Oct. 1982)

VITA

Victor Clark Esch was born in Angola, Indiana on 6 February 1960. He graduated from Hayfield High School, Alexandria, Virginia in 1978. Following this, he attended Purdue University under an ROTC scholarship, graduated in May 1982, and was commissioned in the USAF. After working as a computer programmer in the Washington D.C. area for six months, he reported to Wright-Patterson AFB to work in the Elecro-Optic Sources Group, Electronic Technology Division, Avionics Laboratory. He attended the Air Force Institute of Technology part time from March 1983 to March 1986.

UNCLASSIFIED
SECURITY CLASSIFICATION OF THIS PAGE

AD-A172 783

REPORT DOCUMENTATION PAGE

1a. REPORT SECURITY CLASSIFICATION: UNCLASSIFIED	1b. RESTRICTIVE MARKINGS
2a. SECURITY CLASSIFICATION AUTHORITY	3. DISTRIBUTION/AVAILABILITY OF REPORT: Approved for public release: Distribution Unlimited
2b. DECLASSIFICATION/DOWNGRADING SCHEDULE	
4. PERFORMING ORGANIZATION REPORT NUMBER(S): AFIT/GEP/ENP/85D-11	5. MONITORING ORGANIZATION REPORT NUMBER(S)
6a. NAME OF PERFORMING ORGANIZATION: School of Engineering; 6b. OFFICE SYMBOL (If applicable): AFIT/EN	7a. NAME OF MONITORING ORGANIZATION
6c. ADDRESS (City, State and ZIP Code): Air Force Institute of Technology, WPAFB OH 45433	7b. ADDRESS (City, State and ZIP Code)
8a. NAME OF FUNDING/SPONSORING ORGANIZATION: Avionics Laboratory; 8b. OFFICE SYMBOL (If applicable): AFWAL/AADO	9. PROCUREMENT INSTRUMENT IDENTIFICATION NUMBER
8c. ADDRESS (City, State and ZIP Code): AFWAL/AADO, WPAFB OH 45433-6543	10. SOURCE OF FUNDING NOS.

PROGRAM ELEMENT NO.	PROJECT NO.	TASK NO.	WORK UNIT NO
62204F	2001	05	09

11. TITLE (Include Security Classification): See Block 19	
12. PERSONAL AUTHOR(S): Victor C. Esch, B.S., 1st Lt, USAF	
13a. TYPE OF REPORT: MS Thesis; 13b. TIME COVERED: FROM _____ TO _____	14. DATE OF REPORT (Yr., Mo., Day): 1986 March; 15. PAGE COUNT
16. SUPPLEMENTARY NOTATION	

17 COSATI CODES		
FIELD	GROUP	SUB. GR.
20	06	

18. SUBJECT TERMS (Continue on reverse if necessary and identify by block number): Optics, Phase Conjugation, Laser, Resonator, Stimulated Brillouin Scattering

19. ABSTRACT (Continue on reverse if necessary and identify by block number)

Title: "An Investigation of a Phase Conjugate Resonator Based on Stimulated Brillouin Scattering"

Thesis Chariman: Dr. W. B. Roh

Approved for public release: IAW AFR 190-1.
LYNN E. WOLAVER
Dean for Research and Professional Development
Air Force Institute of Technology (AFIT)
Wright-Patterson AFB OH 45433
9 May 86

20. DISTRIBUTION/AVAILABILITY OF ABSTRACT: UNCLASSIFIED/UNLIMITED XX SAME AS RPT ☐ DTIC USERS ☐	21. ABSTRACT SECURITY CLASSIFICATION: UNCLASSIFIED

22a. NAME OF RESPONSIBLE INDIVIDUAL	22b. TELEPHONE NUMBER (Include Area Code)	22c. OFFICE SYMBOL
Dr. W. B. Roh	(513) 255-4877	AFIT/PH

DD FORM 1473, 83 APR — EDITION OF 1 JAN 73 IS OBSOLETE

UNCLASSIFIED
SECURITY CLASSIFICATION OF THIS PAGE

A phase conjugate resonator (PCR) using stimulated Brillouin scattering (SBS) was investigated. Carbon disulfide, in a waveguide tube, was used as the nonlinear medium. A collinear startup resonator was employed, and output was obtained by cavity dumping the phase conjugate resonator.

The performance of the PCR was optimized through use of etalon elements including resonator reflectors. Aberration and misalignment were used to test the fault tolerance of the PCR.

The PCR compensated well for the introduced faults with respect to energy output, but beam quality was, in general, degraded by the SBS process. The large SBS shift of carbon disulfide hurt the performance of the PCR.

END

11-86

DTIC